CHEMICAL PLANT ANALYSIS OF HYDROGEN PRODUCTION BASED ON THE HYBRID-SULFUR AMMONIA WATER SPLITTING CYCLE

A Thesis

by

ABDUR RAHMAN SHAZED

Submitted to the Office of Graduate and Professional Studies of
Texas A&M University
in partial fulfillment of the requirements for the degree of

MASTER OF SCIENCE

Chair of Committee,	E. Konstantinos Kakosimos
Committee Members,	Ahmed Abdel-Wahab
	Arun R. Srinivasa
Head of Department,	M. Nazmul Karim

December 2017

Major Subject: Chemical Engineering

ABSTRACT

Several types of research are going on for the development of the green hydrogen generation process. One similar effort to produce green hydrogen is the current work. Hydrogen is useful for both mobile and stationary fuel cell purposes. The current solar thermochemical water splitting cycle (TCWSC) can reach an overall efficiency of 35-40%. This efficiency is higher than that of other solar-to-hydrogen generation processes, i.e., PV-electrolysis, photo-electrochemical, photo-catalytic and photo-biological. However, there are some shortcomings that demote feasibility of the current TCWSC for practical application. These shortcomings are (i) the utilization of only the thermal (IR) component of the solar irradiation, neglecting a photonic (UV-Vis) component; (ii) not taking into consideration the intermittent nature of the solar resource; and (iii) the involvement of technically challenging reagents transport and separation stages. The objectives of this current work are to develop a solar water splitting production process that can utilize both the thermal and photonic parts of the solar energy and integrate a thermal energy storage system, which can supply the thermal energy in the absence of sun.

The developed process consists mainly five reactors (a photochemical, three thermochemical & an absorber). This process also has incorporated a thermal energy storage system. This thermal energy storage system utilizes process fluid (molten salts and gasses) to store or supply energy. The process is a total recycle process, as only water is fed to the system for getting hydrogen and oxygen as products and all other materials are contained in the system. The plant was designed to produce 7000 kmol H2/hr that is

equivalent to 476 MW energy based on a lower heating value of hydrogen. The required thermodynamic properties for some species involved in the model were obtained from the literature ,as these compounds' properties are not available in the database of Aspen properties. Moreover, an improved thermodynamic model from literature was used in the simulator to enhance the performance of the developed model. An optimum solar-to-H2 efficiency of 50% was achieved, which is higher than previous attempts (~23%). At the same time, to ensure complete liquid operation of the cycle, literature data of the K2SO4-K2S2O7 phase diagram was incorporated into the model.

The simulation showed for that 1 hour, the thermal energy storage system could keep the temperature of all the reactors at the desired level even without the presence of the sun. This TES absorbs and stores thermal energy from the process while there is more energy than required and supplies energy when there is energy shortage in the process. However, in the absence of the sun, the model will not produce any hydrogen, as there will be no photonic energy at that time, which reduces the efficiency to zero.

The maximum salt flow rate for supplying thermal energy was found to be 330 kmol/kmol of hydrogen and for storing energy was 2139 kmol/kmol of hydrogen. Moreover, the economic analysis indicated that both options, i.e., process with thermal energy storage system and process without thermal energy storage system are economically feasible. The internal rate of returns for the two options are 20.57% and 24.44% consecutively for this two options. The analysis also showed that though the process with TES is not economically feasible, it enables early start-up of the production process and provides production stability.

DEDICATION

To my mother *Thamina Khatun* and my father *Mashiullah* for their unconditional love and support. And to my lovely wife for her love, understanding, and support.

Acknowledgement

CONTRIBUTORS AND FUNDING SOURCES

This work was supervised by a thesis committee consisting of Assistant Professor Dr. Konstantinos Kakosimos (chair) and Professor Dr. Ahmed Abdel-Wahab of Chemical engineering department of Texas A&M University at Qatar and Professor Dr. Arun Srinivasa of the department of mechanical engineering at Texas A&M University, College station. Each of the committee members helped and guided me whenever I asked for any help regarding the simulation or direction of workflow.

Dr. Konstantinos's guidelines in each weekly meeting with him helped me to follow the correct path in reaching the objectives of the study. He also helped me in reproducing the phase diagram showed in Figure-2.

Agni Kalyva, a graduate student and member of SCARELAB research group, taught me to manually incorporate heat capacity parameters mentioned in section 3.1.2 in Aspen plus.

This publication was made possible by a NPRP award [NPRP 6 - 116 - 2 - 044] from the Qatar National Research Fund (a member of The Qatar Foundation). The statements made herein are solely the responsibility of the authors. The HPC resources and services used in this work were provided by the IT Research Computing group at Texas A&M University at Qatar. IT Research Computing is funded by the Qatar Foundation for Education, Science, and Community Development.

NOMENCLATURE

TWSC	Thermochemical Water Splitting Cycle
TES	Thermal Energy Storage
P	Pressure
T	Time
LTR	Low-Temperature Reactor
MTR	Mid-Temperature Reactor
HTR	High-Temperature Reactor
TES	Thermal Energy Storage

TABLE OF CONTENTS

LIST OF FIGURES

Page

LIST OF TABLES

Page

1. INTRODUCTION

Use of fossil fuels has become a greater concern in recent time mainly because of environmental issues. Therefore, the quest for an environmentally friendly source of energy becomes prevalent. There are many growing areas of study on the sustainable energy sources such as hydroelectric, wind, geothermal, biomass, solar photovoltaic, solar thermal, and solar-photo-thermal, etc.[1]. Each of these sources has its pros and cons. This work focuses on using solar energy, where the solar photo and thermal energy is used separately to produce Hydrogen.

Extended research work has been conducted on developing a feasible production process for hydrogen. The water splitting into hydrogen and oxygen can be performed in a single step, but this requires very high temperature (4700 K) [2]. Hydrogen can also be generated from many energy sources using a range of processes including reforming of natural gas, gasification of coal, and electrolysis of water into hydrogen and oxygen using electricity. Although such processes are commercially available, alternative processes are under development. Some of these alternatives use Thermochemical water splitting cycles (TWSC). In TWSC, unlike single step decomposition, water is decomposed into hydrogen and oxygen through a series of intermediate reactions. Water and heat are the inputs, and hydrogen and oxygen are the outputs from a TWSC. The other chemicals and reagents are recycled in a closed cycle.

The required energy for water splitting process can be obtained from many sources like nuclear, electrical, or renewable, etc. However, the process will be much more environmentally acceptable if we can utilize concentrated solar energy. TWSC

involves two steps i.e. Hydrogen generation sub-cycle and Oxygen generation sub-cycle [3].

There is a number of TWSC studied so far, such as metallic oxides cycle, a mixture of metallic oxides cycle, hybrid sulfur-iodine cycle, etc. In addition to having disadvantages like high operating temperature, critical separation process, sintering, deactivation, etc., all these TWSC suffers one common drawback they can only utilize the thermal part of the solar energy. Thus, all these TWSC neglect the quantum component of the solar energy. These processes do not also consider the intermittent nature of solar energy. The availability of the sun is only twelve hours, and the heat flux varies from hour to hour.

To mitigate the mentioned drawbacks this work focuses on the design and analysis of a hydrogen production process based on a novel hybrid water-splitting cycle [4]. This cycle involves a solar-photo-chemical hydrogen generation step and a high-temperature solar-thermo-chemical oxygen generation step and uses Ammonia as a working reagent and an alkali metal as mediator.

Furthermore, besides design and analysis of the hydrogen production process, this study focusses on the integration of a thermal storage system to make the process operation independent of the intermittent nature of solar energy. The thermal energy storage system can store the surplus energy as sensible heat and supply heat energy from storage when there is an energy shortage during the process operation.

Therefore, the objectives of this research work include but not limited to development of the preliminary chemical process flowsheet, Process heat, and mass

balance, process optimization, and heat transfer analysis of solar reactor. The scope also includes the feasibility analysis of a thermal energy storage system for 24 hours operation and an economic analysis of the process to evaluate the economic feasibility of the process with thermal energy storage system.

1.1. Literature review

There are many long existing processes for the generation of hydrogen, like reforming of natural gas, gasification of coal, electrolysis, etc. However, since concern for environment and preference for green energy use has risen in recent past, research for alternative processes continued. One of these alternatives is thermochemical water decomposition, in which water decomposes into hydrogen and oxygen through intermediate reactions.

One approach can involve the use of nuclear energy to deliver the energy required for operation of the thermochemical water decomposition process. Another approach for hydrogen production can be the utilization of solar energy as the primary energy input [1]. There are more than 280-referenced cycles out of which 30 cycles are under intense investigation [2].

The thermochemical water splitting is a chemical process that performs the multi-step decomposition of water. Hydrogen can also produce by reforming or electrolysis, but alongside causing damage to the environment, these processes suffer thermodynamic inefficiencies. The projected current combined efficiency for electrolysis does not exceed 36%. On the other hand, the overall efficiency of most investigated

Thermochemical Water Splitting Cycle (TWSC) have expected to be 40-50%, without the intermediate production of electricity. [2].

Solar energy can utilize for the generation of hydrogen in two processes, one by direct decomposition and the second one is by TWSC.

In the first method, i.e. direct decomposition involves very high operating temperature. Recently the development of highly efficient solar concentrator enables to achieve temperature as high as 3400°C [5]. This efficient solar contractor allows direct utilization of solar energy for thermal decomposition of water into hydrogen and oxygen in one steps according to the following reaction.

$$\mathbf{H_2O \leftrightarrow H_2 + {}^{1}\!/_{2}\, O_2} \quad \left(\Delta \mathbf{H = 284 \frac{KJ}{mole} H_2}\right) \qquad \mathbf{(1)}$$

The required temperature for direct thermolysis of water is greater than 2800K. At this temperature, the decomposition yield of water is about 10% (ΔG=0 at 4700K). Also, the product must be quenched to prevent hydrogen and oxygen from recombining during cooling [2]. The high-temperature requirement, a minuscule percentage of yield and complicated separation process has made this direct decomposition process less feasible.

On the other hand, the thermochemical water splitting cycle (TWSC) consists of the conversion of water into hydrogen and oxygen by a series of endothermic and exothermic chemical reactions. The endothermic reaction can run by solar thermal energy. The TWSC involves mainly two steps-cycle based on metallic oxides, such as MO_{OX}/MO_{red} where M symbols a metal such as Zn, Fe, Mo, Si, etc.[6]. A significant number of redox pairs have been considered so far, among which Zn/ZnO and iron-

based oxide $(Fe_{1-x}M_x)_3O_4/(Fe_{1-x}M_x)_{1-y}O$ are the most promising redox working materials that have intensively investigated. New redox pairs, such as SnO_2/SnO, CeO_2/CeO_3, GeO_2/GeO, MgO/Mg, etc., have also been proposed recent years [3].

Thermochemical cycles are used to achieve water splitting because they allow production of appreciable amounts of hydrogen and oxygen at much lower temperatures (usually below 1000°C) than the temperature needed for direct one-step thermal water decomposition [1]. Few examples of such cycle reactions are

- Fe_3O_4/FeO cycle [7]:

Oxygen half cycle:

$$\mathbf{Fe_3O_4 \rightarrow FeO + {}^{1}/_{2}\, O_2} \qquad \mathbf{(2)}$$

- Hydrogen half cycle:

$$\mathbf{3FeO + H_2O \rightarrow Fe_3O_4 + H_2} \qquad (3)$$

(Maximum temperature involved 2200°C)

- Zn/ZnO cycle [2]:

Oxygen half cycle:

$$\mathbf{ZnO \rightarrow Zn + {}^{1}/_{2}\, O_2}, (2000°\mathbf{C}) \qquad (4)$$

Hydrogen half cycle:

$$\mathbf{Zn + H_2O \rightarrow ZnO + H_2}, (1100°\mathbf{C}) \qquad (5)$$

Despite having advantages like relatively high theoretical hydrogen yield and the competence to avoid the recombination of hydrogen & oxygen and also to avoid irreversibility associated with quenching needed with volatile metal oxides, the Fe_3O_4/FeO cycle has a significant disadvantage such as severe sintering and melting

occurred during thermal decomposition of Fe_3O_4 with strong vaporization. Moreover, rapid deactivation occurs of the iron oxide particles during the cyclic reaction and milling or granulation required for obtaining reasonable conversion for the hydrolysis of FeO. The Zn/ZnO cycle has slit lower activation temperature than Iron oxide cycle and potentially high exergy conversion efficiency (29%) but still, the temperature is too high and needs fast quenching to minimize Zn recombination, and sintering still exists [3].

Thus curtail of the operating temperature has become the primary objective of future research. One such effort is the partial substitution of iron in iron oxide with other metal oxides. Such as partial substitution of iron in Fe_3O_4 by M_3O_4/MO (M =Mn, Co, Mg, Ni, Zn, etc.) is possible to form mixed metal oxides $(Fe_{1-x}M_x)_3O_4$ which may be reducible at a lower temperature whereas the reduced phase still capable of performing the hydrolysis reaction. An example of one such cycle is $MnFe_2O_4/NaCO_3/NaMn_{1/3}Fe_{2/3}O_2$ composite system which involves following reactions.

1. Activation step (873-973K):

$$\mathbf{6Na(Mn_{1/3}Fe_{2/3}O_2) + 3CO_2 \rightarrow 2MnFe_2O_4 + 3Na_2CO_3 + {}^{1}/_{2}\,O_2} \quad \textbf{(6)}$$

2. Hydrolysis step (973K):

$$\mathbf{2MnFe_2O_4 + 3Na_2CO_3 + H_2O \rightarrow 6Na\left(Mn_{1/3}Fe_{2/3}O_2\right) + 3CO_2 + H_2,} \quad \textbf{(7)}$$

This system has significantly low operating temperatures and the potential for high efficiency in the range of 42-68% varying as a function of quantities of utilized carrier gas. But the mixture rapidly passivated and unable to further produce hydrogen after a few cycles [3].

There are some other different types of cycles that utilize metal halide and metal sulfate. Several factors have considered before sorting this metal halide and metal sulfate cycles like availability and abundance of materials, simplicity, chemical viability, thermodynamic feasibility and associated safety issues. Considering all these factors eight cycles have identified as of possible commercial significance: sulfur-iodine (S-I), copper-chlorine (Cu-Cl), cerium-chlorine (Ce-Cl), iron-chlorine (Fe-Cl), magnesium-iodine (Mg-I), vanadium-chlorine (V-Cl), copper-sulfate (Cu-SO_4) and hybrid chlorine. All of this process requires operation temperature above 800°C except the Cu-Cl cycle (around 530°C) [8]. These cycles follow a five steps reaction procedure:

1. Hydrogen production step (450°C)

$$\mathbf{2Cu_{(s)} + 2HCl \rightarrow 2CuCl_{(l)} + H_{2(g)}} \quad (8)$$

2. Electrolysis step (Ambient temperature)

$$\mathbf{2CuCl_{(aq)} \rightarrow 2CuCl_{2(aq)} + 2Cu_{(s)}} \quad (9)$$

3. Drying step (70°C)

$$\mathbf{2CuCl_{2(aq)} \rightarrow 2CuCl_{2(s)}} \quad (10)$$

$$\mathbf{2CuCl_{2(slurry)} \rightarrow 2CuCl_{2(s)}} \quad (11)$$

$$\mathbf{2.2H_2O_{(l)} \rightarrow 2.2H_2O_{(g)}} \quad (12)$$

$$\mathbf{0.1HCl_{(aq)} \rightarrow 0.1HCl_{(g)}} \quad (13)$$

4. Hydrolysis step (375°C)

$$\mathbf{2CuCl_{2(s)} + H_2O_{(g)} \rightarrow CuO.CuCl_{2(s)} + 2HCl_{(g)}} \quad (14)$$

Oxygen production step (530°C)

$$\mathbf{CuO.CuCl_{2(s)} \rightarrow 2CuCl_{(l)} + {}^{1}/_{2}\, O_2} \quad (15)$$

Though this is a very promising cycle for the production of hydrogen with a realistic thermal efficiency of 43%, it has some major drawbacks. Besides having complex separation process, at 530°C temperature, the unconverted chlorine can corrode the equipment. Also at the low operating temperature effective catalysis is a big challenge [9].

Japan Atomic Energy Agency (JAEA) is performing research and development on the thermochemical water splitting iodine-sulfur process for hydrogen production with the use of heat from a nuclear reactor process plant. This cycle follows the following series of reactions

1. $\mathbf{I_2 + SO_2 + 2H_2O \rightarrow 2HI + H_2SO_4}$ (16)
2. $\mathbf{H_2SO_4 \rightarrow H_2O + SO_2 + {}^{1}/_{2}\, O_2}$, (900-1000°C) (17)
3. $\mathbf{2HI \rightarrow H_2 + I_2}$ (18)

JAEA has addressed some IS process thermal efficiency degradation issues. The hydrogen production thermal efficiency in the bench-scale experiment was less than 10% due to the substantial heat loss in the HI separation step. With extractive distillation, a reported thermal was 47%, but the chemical used appears to be very corrosive. Realistic thermal efficiency using membrane application has reported being 34% [10]. This process requires high temperature than some competing processes and is still under development. In IS cycle I_2 is present in both step 1 and 3. The separation of iodine from other gasses is very challenging because I_2 present as a gas when the

temperature is higher than 373K. Also, I_2 is characterized by strong sublimation, which makes the solidification separation method not reliable and stable [11].

However, along with individual disadvantages, all of these processes have one major drawback; all of the above-discussed processes are competent to use only the thermal portion of solar light. Solar light has two sets of energies in it, the thermal and the photonic energy. All the processes mentioned above can only utilize the thermal portion neglecting the potential of photonic energy. Thus, if a process can incorporate this photonic energy, then its overall efficiency will improve for sure.

To overcome this flaw in the use of energy, a novel sulfur-ammonia (S-A) cycle has developed at Florida Solar Energy Center (FSEC) by A.T-Raissi and his team. In the FSEC's S-A cycle, the Gibbs energy was supplied to the cycle via photons (at wavelengths greater than 350 nm), thus making it compatible with a solar power source [4]. It has the following steps

Chemical absorption, (300K)

$$\mathbf{SO_{2(g)} + 2NH_{3(g)} + H_2O_{(l)} \rightarrow (NH_4)_2SO_{3(aq)}} \quad (19)$$

Photo-chemical steps, (350K)

$$\mathbf{(NH_4)_2SO_{3(aq)} + H_2O_{(l)} \rightarrow (NH_4)_2SO_{4(aq)} + H_{2(g)}} \quad (20)$$

Thermochemical steps, (550K)

$$\mathbf{H_2SO_{4(l)} + (NH_4)_2SO_{4(aq)} \rightarrow H_2O_{(g)} + 2NH_{3(g)} + H_2S_2O_{7(l)}} \quad (21)$$

Thermochemical steps, (1125K)

$$\mathbf{SO_{3(g)} \rightarrow SO_{2(g)} + {}^{1}/_{2}\, O_{2(g)}}) \quad (22)$$

But since all sulfur family thermochemical water splitting cycle relies on concentration and decomposition of sulfuric acid for the oxygen evolution step of the cycle, the sulfuric acid decomposition step presents serious materials and catalyst deactivation challenges. To overcome this Florida solar center has developed some pure solar driven sulfur ammonia based TWSCs in which high photonic energy is used for the photocatalytic production of H_2 based on the photochemical oxidation of aqueous SO_3^{2-} ions. The remaining portion of solar thermal energy is utilized for production of O_2 via decomposition of metal sulfates (MSO_4) or metal pyro-sulfates. [4] The main advantages of the proposed S-A cycle are

- The S-A cycle includes a step wherein the energy of solar photons is directly converted into the chemical energy of hydrogen without using the intermediate devices such as photovoltaic cells.
- No electrical energy input is required and
- Maximum temperature involved is 1125 K

One such process evaluated by Science Applications International Corporation (SAIC) with the support of the University of California San Diego, Electrolysis Company, Inc. and Thermochemical Engineering Solutions based on a sulfur ammonia (SA) cycle for splitting water to produce hydrogen. This cycle consists of a molten salt sub-cycle as follows [12]

Chemical absorption (298-323K)

$$\mathbf{SO_{2(g)} + 2NH_{3(g)} + H_2O_{(l)} \rightarrow (NH_4)_2SO_{3(aq)}} \quad (23)$$

Electrolytic oxidation (353-423K)

$$(NH_4)_2SO_{3(aq)} + H_2O_{(l)} \rightarrow (NH_4)_2SO_{4(aq)} + H_{2(g)} \quad (24)$$

Adiabatic mixing (673-723K)

$$K_2SO_{4(l)} + (NH_4)_2SO_{4(aq)} \rightarrow H_2O_{(g)} + 2NH_{3(g)} + K_2S_2O_{7(l)} \quad (25)$$

Solar thermal (1063K)

$$K_2S_2O_{7(l)} \rightarrow SO_{3(g)} + K_2SO_{4(l)} \quad (26)$$

Electric heat (1123-1473K)

$$SO_{3(g)} \rightarrow SO_{2(g)} + {}^{1}/_{2}\, O_{2(g)} \quad (27)$$

They investigated this cycle using aspen plus process simulator with the production of 1.7 X 105 kg H2/day. The developed model does not have any gas-gas and gas-liquid separation steps in it. Simplicity in separation is an advantage as less than 1% energy is consumed for separation. The drawbacks their analysis have are: (1) It involves higher operating temperature than the competing processes. (2) the resulted efficiency is very low (13%) and finally (3) it does not have any provision to utilize both components of solar energy.

Littlefield and his team [13] also used AspenPlus© process simulator for process modeling and thermochemical analysis of this same cycle with an electrolyzer in the system. According to his model and analysis, a mixture of potassium sulfate and potassium pyrosulfate lowers the melting point of the solution by 100°C and solution is liquid at around 350°C. In his simulation, Littlefield performed all the reactions according to following specified temperature.

Chemical absorption (25°C)

$$SO_{2(g)} + 2NH_{3(g)} + H_2O_{(l)} \rightarrow (NH_4)_2SO_{3(aq)} \quad (28)$$

Electrolytic oxidation (80-150°C)

$$(NH_4)_2SO_{3(aq)} + H_2O_{(l)} \rightarrow (NH_4)_2SO_{4(aq)} + H_{2(g)} \quad (29)$$

Solar thermal (400°C)

$$K_2SO_{4(l)} + (NH_4)_2SO_{4(aq)} \rightarrow H_2O_{(g)} + 2NH_{3(g)} + K_2S_2O_{7(l)} \quad (30)$$

Solar thermal (835°C)

$$K_2S_2O_{7(l)} \rightarrow SO_{3(g)} + K_2SO_{4(l)} \quad (31)$$

Solar thermal (1000°C)

$$SO_{3(g)} \rightarrow SO_{2(g)} + {}^{1}/_{2}\, O_{2(g)} \quad (32)$$

According to Littlefield's process model, the overall efficiency of the plant is 23% which can be increased with further research into more improved heat integration and different mode of power generation. The AspenPlus® model proves the viability of the process.

One purpose of this process i.e. the complete dependency on solar energy has not been analyzed as Littlefield investigated the process with AspenPlus® process simulator using an electricity driven electrolyzer. Thus, this novel process with photochemical steps requires being investigated further.

An investigation of the novel HySA TWSC with modified thermodynamics indicates that favorable conversion to the product can be achieved at a lower temperature than the temperature used by Littlefield. According to the study, reaction-31 and-32 take place at 550°C and 850°C instead of 835°C and 1000°C and a higher theoretical efficiency of 60% was achieved [14,15].

Zhang and his team [16], investigated the metal/metal oxide cycle using TiO2 photocatalyst. In this cycle, the process by which metal oxides reduce through concentrated solar energy is replaced with a photochemical reaction while water still dissociates via a thermos-chemical reaction. Thus photo-thermochemical cycles that combine these two reactions can initiate at relatively low temperatures, unlike thermochemical cycles operated at extremely high temperatures in all the metal/metal oxide cycle. These reactions can express as

$$\mathbf{M_xO_y = M_xO_{y-1} + {}^{1}/_{2}\, O_{2(g)}}\text{; (photochemical reaction, room temperature)} \quad (33)$$

$$\mathbf{M_xO_{y-1} + H_2O = M_xO_y + H_{2(g)}}\text{; (Thermochemical reaction, 500-600°C)} \quad (34)$$

(Where M_xO_y represents TiO_2 and M_xO_{y-1} represents photo reduced TiO_2)

For most of the metal oxides pair, before the required thermochemical reaction temperature was above 1200°C. But by the use of photocatalyst, the first reaction now takes place at room temperature. Therefore, the maximum operating temperature has become 600°C [16].

Though the introduction of the photocatalyst to absorb photonic energy is a massive improvement to the TWSC of metal/metal oxides cycle, the rate of production of hydrogen is very low i.e. 0.4 mL of hydrogen was produced for 60 minutes of irradiation for per gram of 600°C -heated TiO_2.

The second major drawback of solar powered cycles is the intermittent nature of solar energy. Running these processes smoothly, when solar energy fluctuates require a separate source of energy. A part of solar energy can be stored to form a separate source or storage of thermal energy when solar heat energy is more than required. Then we can

supply thermal energy from this storage when there is a shortage of energy for process operation.

Solar energy can be stored as mechanical energy, chemical energy, electrostatic energy, magnetic energy, biological energy for a long or short period. All these mentioned means of storing energy has an individual level of energy penalties like in mechanical energy storage system only 50% of the stored energy is recoverable [17]. Similarly, in the case of chemical energy storage system (Batteries), the energy delivery rate is slow compared to other processes thus not acceptable [18]. Electrostatic energy storage system uses capacitors to store energy. This storage system is suitable as short-term buffer storage and incompetent for bulk energy storage. There are some significant advantages of magnetic energy storage system, but the energy densities available from this technology are not yet comparable to the amounts achieved through chemical batteries. The biological energy storage is still under development [17].

All these energy storage systems discussed so far can only store solar energy by converting it into either electrical or mechanical energy thus suffers significant energy conversion losses.

Thermal part of Solar energy can also be stored as heat energy. When energy is stored as heat or thermal energy is called thermal energy storage (TES). TES system store available thermal energy directly without converting energy to electricity. The three main types of thermal energy storage system are sensible heat, latent heat, and thermo-chemical heat [19].

Sensible heat is the simplest method to store thermal energy and consists of applying a temperature gradient to a media (solid or liquid) to accumulate or release heat. Sensible TES technologies are usually low in cost and are one of the current most popular TES technologies [20]. More than 90% of all thermal energy storage processes used in a wide range of applications are sensible heat storage process [21] However, these storage systems provide very low energy densities, between 10 and 50 kW h/m3 [17]. Some of the main disadvantages of low energy densities include the need for large storage volumes, as well as large storage containers. Also, this means of energy storage suffers significant heat losses to the significant this loss can lower storage efficiency despite having this disadvantages up to now, low cost and simplicity of design have made operational process relied on sensible heat TES [22].

In latent heat TES Phase change material (PCM), stores and releases heat at a particular required temperature as it undergoes a phase change at that temperature [23]. The use of a latent heat storage system using phase change materials (PCMs) is an effective way of storing thermal energy and has the advantages of high-energy storage density and the isothermal nature of the storage process. Latent heat TES can store 5–14 times more heat per unit volume than sensible heat TES [24]. PCMs are usually classified as organic (paraffin, fatty acids, alkanes) or inorganic (salts) [25,26]. Organic PCMs have no corrosives and have chemical and thermal stability, but they have lower phase chang enthalpy, low thermal conductivity, and inflammability. On the other hand inorganic, PCMs has high phase change enthalpy but has less chemical and thermal stability. Organic compounds operating temperature range i.e. melting point varies from

4.5°C to 145°C but operating temperature range for the inorganic compound span from 48°C to 897°C [26].

R. Taylor [12] demonstrated with aspen plus process simulator the use of a phase change thermal storage system with NaCl salt as the process fluid this storage system can work at 1073 K temperature. One disadvantage of this thermal storage system is it requires handling both solid and liquid salts. In addition to that, it requires handling two distinct types of salts i.e. metal sulfate and chloride salt, which means more capital investments.

In thermo-chemical TES, energy is stored through a reversible reaction and then recovered when the reaction is reversed. By storing energy in the form of chemical bonds of suitable materials, energy can be stored with almost no energy loss for long periods of time. At the same time, high energy storage density can be achieved. Both criteria are crucial for future energy storage applications. The range of operating temperature for thermochemical energy storage varies from 100°C to 950°C at which [28]. Although chemical reaction can provide high energy densities, they often require a catalyst to release the heat and control the reaction and thus are not always desirable [17].

Furthermore, despite the large potential of chemical and latent mechanisms, further research and development are required for these concepts to result in reliable and economically competitive thermal energy storage systems [25].

This study focusses on integrating a thermal energy storage system with the solar hydrogen production process. This storage system should store thermal energy using

process fluid. TES using process fluid will help us in keeping the simplicity of the process and involve less capital investment. Only sensible thermal energy storage with process fluid (potassium salt) meets our requirements out of the three TES.

Thermal energy storage capacity is calculated by the ratio of energy delivered to energy input. This efficiency and cost of the TES system depend on following factors [27].

1. The thermal capacity of the storing fluid.
2. Thermal loss from the storage system.
3. Power requirement for the addition or removal of heat.
4. Stable chemical properties.

The existing sensible thermal energy storage systems are mainly, active direct storage system.(in which thermal energy is stored as steam) [28], thermocline (stored thermal energy in rock, sand, and oil) [29], oil (a mineral oil called caloria, specially designed for this purpose) [30], molten salt ($NaNO_3$ and KNO_3) [31].

In this current work, we will investigate the performance of molten potassium sulfate-pyrosulfate salt and its feasibility of this thermal energy storage system as an integrated part of solar sulfur-ammonia hydrogen production process.

Thus, there is a need to develop such a solar thermochemical water splitting cycle that can utilize both photonic and thermal part of solar energy with an integrated thermal energy storage system for round the clock operation.

1.2. Solar hybrid sulfur-ammonia process

The solar hybrid sulfur ammonia process (HySA) takes place in two sub-cycles: oxygen generation and hydrogen generation. In total, these two sub-cycles include the following five reactions

1. Oxygen sub-cycle:

   Thermochemical 400°C

   $$\mathbf{K_2SO_4 + (NH_4)_2SO_4 \rightarrow H_2O + 2NH_3 + K_2S_2O_7} \quad (35)$$

   Thermochemical 550°C

   $$\mathbf{K_2S_2O_7 \rightarrow SO_3 + K_2SO_4} \quad (36)$$

   Thermochemical 850°C

   $$\mathbf{SO_3 \rightarrow SO_2 + {}^{1}/_{2}\, O_2} \quad (37)$$

2. Hydrogen half-cycle:

   Chemical absorption 25°C

   $$\mathbf{SO_2 + 2NH_3 + H_2O \rightarrow (NH_4)_2SO_3} \quad (38)$$

   Photochemical 80°C

   $$\mathbf{(NH_4)_2SO_3 + H_2O \rightarrow (NH_4)_2SO_4 + H_2} \quad (39)$$

A T-Raissi [4] of Florida Solar Energy Centre has originally developed this HySA. Figure 1 shows a schematic block diagram of this cycle.

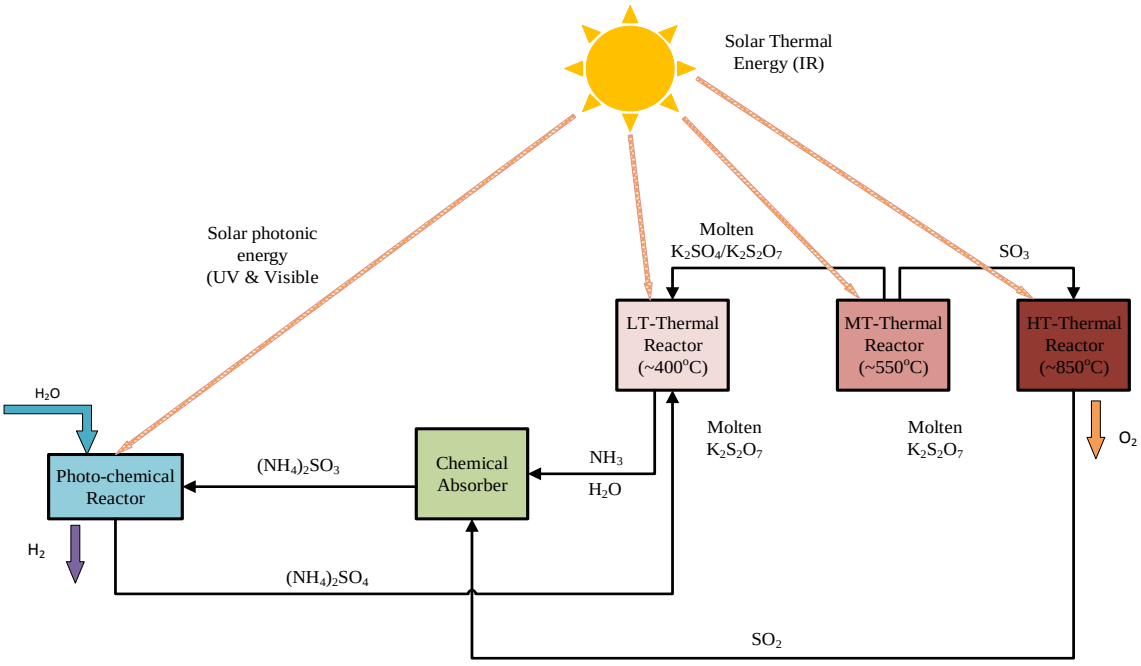

Figure 1: A Schematic block diagram of photo-thermo-chemical solar hybrid sulfur ammonia (HySA) water splitting cycle.

Reaction 35, 36 and 37 consecutively takes place in LTR, MTR, and HTR. In these three reactors section, the input is a mixture of molten salts of potassium sulfate, potassium pyrosulfate, ammonium sulfate and solar thermal energy. The output from this section are ammonia, sulfur trioxide, sulfur dioxide and oxygen.

Reaction 38 takes place in the absorber, and the final reaction (reaction 39) takes place in the photochemical reactor. In the absorber ammonia and sulfur trioxide are absorbed to form ammonium sulfate at 25°C. The photochemical hydrogen formation reaction takes place in the photoreactor. Here reaction is run by photonic energy at 80°C.

2. OBJECTIVES

The main strategic objective of the work is to develop a unique hydrogen production process independent of the use of any fossil fuels. The developed process must be capable of utilizing both parts of solar energy i.e. thermal and solar. The second objective is to include a thermal energy storage system to ensure round the clock operation of the process. In addition to these two primary objectives, this work also intends to perform an economic analysis of the overall process to find the feasibility of the process with integrated thermal energy storage system.

3. METHODOLOGY

To meet the research objectives Aspen Plus chemical process simulator version 8.6 was used in designing the flow sheet for this hybrid SA solar photo-thermo-chemical water splitting cycle. Aspen Plus is a modeling environment for conceptual design, optimization, and performance monitoring for many industries including chemical industries. Aspen Plus uses thermodynamic models that govern the equilibrium relations for the simulated reactors, and these thermodynamic models are assimilated into the program.

In general, we used Non-Random-Two-Liquid (NRTL) model as physical property method in Aspen Plus. Because a variety of forces act on real mixtures, making it difficult to predict the properties of such solutions. Non-ideal solutions are identified by determining the strength and specifics of the intermolecular forces between the different molecules in that particular solution. The NRTL model can describe Vapour Liquid Equilibrium (VLE) and Liquid-Liquid Equilibrium (LLE) of strongly nonideal solutions. The model requires binary parameters. Many binary parameters for VLE and LLE, from literature and regression of experimental data, are included in the Aspen Physical Property System databanks.

Development of the process flow sheet was started first by specifying the design capacity as 7000 kmol/hr H_2 and operating hour to be 12 hours per day. After that, all the essential blocks were identified. Then each of this individual blocks were connected to form the final process flow sheet. In doing so, we faced two challenges one was to ensure complete liquid operation and the second one was converging different blocks.

However to ensure complete liquid operation we took the help of the phase diagram of K_2SO_4-$K_2S_2O_7$ from literature [32]. First, we digitized this phase diagram and found out the equation for each equilibrium line. We used this equation in FORTRAN window of Aspen Plus to force the process simulator to follow these lines for conversion in reactors and maintaining liquid compositions. Figure-2 is showing this phase diagram with different phase regions.

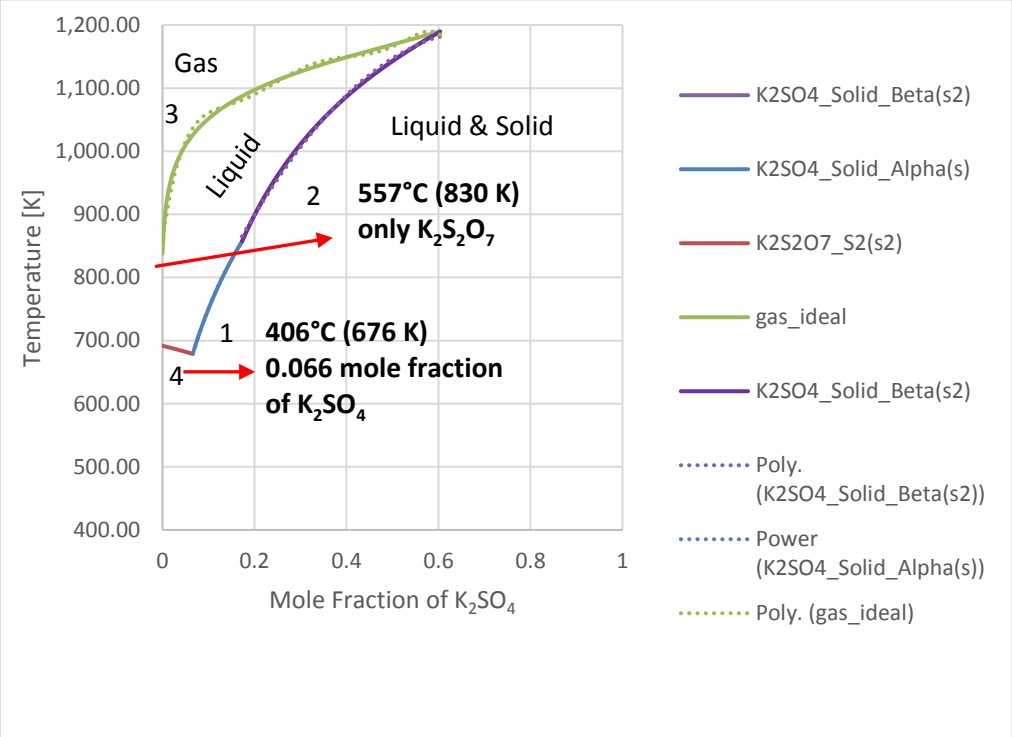

Figure 2: Phase diagram of K_2SO_4-$K_2S_2O_7$ salts.

The percentage of K_2SO_4 will go down from the point of the feed stream of LTR to MTR. Therefore, Aspen was forced to maintain a mole fraction of K_2SO_4 in the feed stream to LTR that is on the line-1. To do so a trend line equation from Microsoft Excel

for line-1 was used in a design specification block in Aspen Plus. Similarly, Aspen was forced to follow line-3 to determine the conversion of $K_2S_2O_7$ in MTR (reaction (36)).

From this phase diagram, we can also see that the lowest temperature of the liquid region and gas region is 406°C and 557°C consecutively. Therefore, the LTR should operate above 406°C temperature, and MTR should operate above 557°C temperature. However, in the case of MTR, we must simulate the reactor at well above 557°C to have a considerable amount of conversion.

The second issue i.e. difficulty in converging different blocks was solved by first converging each block separately. Once the block-by-block flow sheets were converged, then these individual flow sheets can be connected one at a time. Then that connected flow sheet was converged and a new block was connected with this converged flow sheet. And this new flow sheet was converged again. By repeating this process several times, the final converged flow sheet was formed.

After converging the final flow sheet different flow sheet sensitivity analysis, model analysis and calculation was performed. The preceding sections will elaborate all the involved steps in developing the process flow sheet and different analysis of the model in details.

3.1. AspenPlus model properties

Aspen plus properties window helps to define components, reactions, physical, chemical and thermodynamic data. In addition, we can define the basic simulation and flowsheet specifications such as units, yearly operational hours, surrounding temperature, error tolerance for convergence, the maximum number of iterations for

convergence, etc. in Aspen plus properties window. Defining properties is the first step in mathematical process modeling. The following sections will describe in detailed how we specified components, chemistry and thermodynamic properties in Aspen Plus.

3.1.1. General chemistry

The photo-thermo-chemical S-A process constitutes from two sub-cycles; the photocatalytic hydrogen production and the molten salt thermochemical oxygen production. Before defining reactions of the SA cycle, all the involved components were selected from the component specification option in the property window. Figure-3 is showing the list of components used in the simulation.

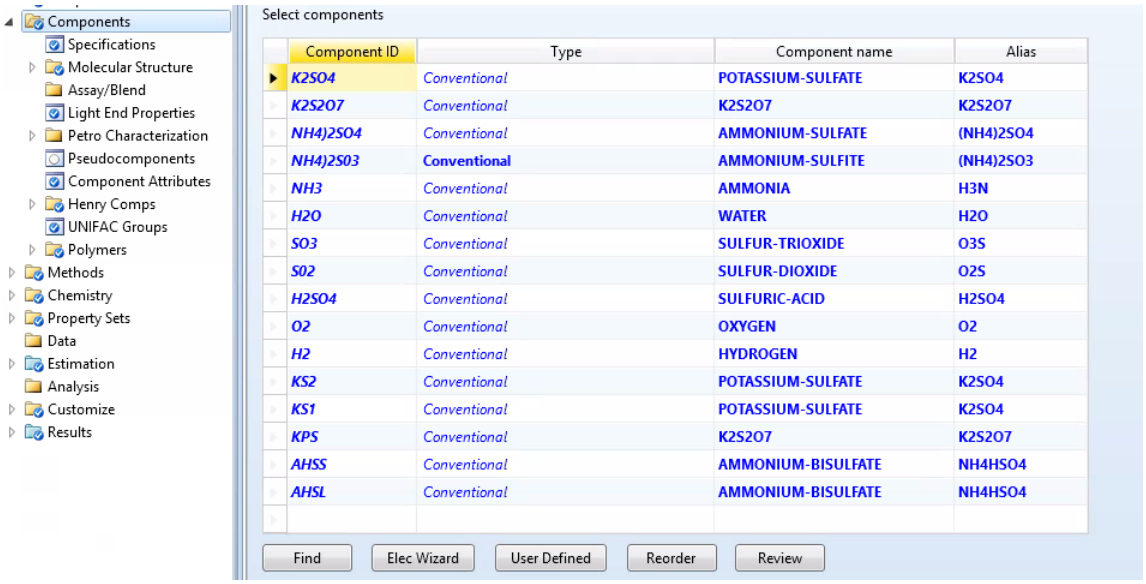

Figure 3: Location of components in the property data browser and specified components.

In our simulation, though we forced Aspen to stay in the liquid region we did not neglect the possibility of solid formation in anywhere of the process flow sheet. Thus, we also considered solid components. In the component list KS1, KS2, KPS, and AHSS represent solid salts in the system.

3.1.2. Thermodynamic model and data input

Since no ions are involved in the process, we chose Non-Random-Two-Liquid (NRTL) property model as it is recommended for non-ideal chemical systems.

Aspen has chemical, physical and thermodynamic properties for most of the components in its database. Only properties for few component i.e. K_2SO_4, $K_2S_2O_7$, $(NH)_4SO_4$, $(NH)_4SO_3$, KS1, KS2, KPS, AHSS, and AHSL were specified manually. These thermodynamic properties are reference state enthalpy, reference state Gibbs energy and heat capacities for both liquids and solids. The preceding section will describe how these properties were set in Aspen properties.

3.2.1.1. Reference enthalpy and Gibbs energy

The reference state for thermodynamic properties is the constituent elements in an ideal gas state at 298.15 K and 1 atm. To calculate enthalpies, entropies and Gibbs free energies Aspen uses:

- Ideal gas heat of formation (DGFORM)
- Ideal gas Gibbs free energy of formation (DGFORM)
- Standard solid heat of formation (DHSFRM)
- Standard solid Gibbs free energy of formation (DGSFRM)

Some of these thermodynamic properties were obtained from the literature [33] Figure-4 shows how and where in property data browser these reference state, thermodynamic properties were added into the model.

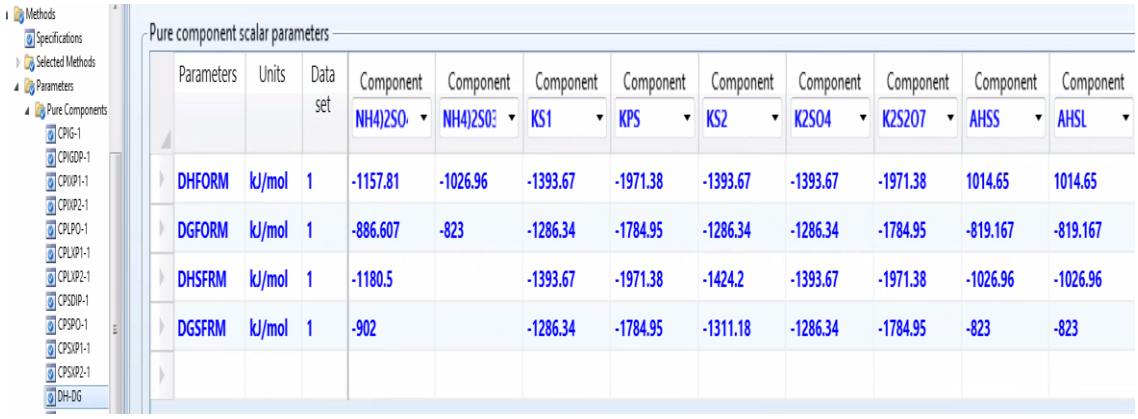

Parameters	Units	Data set	Component NH4)2SO4	Component NH4)2S03	Component KS1	Component KPS	Component KS2	Component K2SO4	Component K2S2O7	Component AHSS	Component AHSL
DHFORM	kJ/mol	1	-1157.81	-1026.96	-1393.67	-1971.38	-1393.67	-1393.67	-1971.38	1014.65	1014.65
DGFORM	kJ/mol	1	-886.607	-823	-1286.34	-1784.95	-1286.34	-1286.34	-1784.95	-819.167	-819.167
DHSFRM	kJ/mol	1	-1180.5		-1393.67	-1971.38	-1424.2	-1393.67	-1971.38	-1026.96	-1026.96
DGSFRM	kJ/mol	1	-902		-1286.34	-1784.95	-1311.18	-1286.34	-1784.95	-823	-823

Figure 4: Location of manual input for properties reference enthalpy and Gibbs energy for $(NH_4)_2SO_4$, $(NH_4)_2SO_3$, KS1, KS2, K_2SO_4, $K_2S_2O_7$, AHSS, and AHSL.

3.2.1.2. Heat capacities

Aspen has several model equations for heat capacities. For two solid state and one liquid state of potassium sulfate (KS1, KS2, and K_2SO_4) we used a model that was based on Barin equation i.e. CPLXP1 and CPLXP2. Two model of heat capacity for the same component is to define heat capacities of that component but for two different temperature range. Figure-5 &-6 is showing how these heat capacity models were set and what were the values for different model parameters.

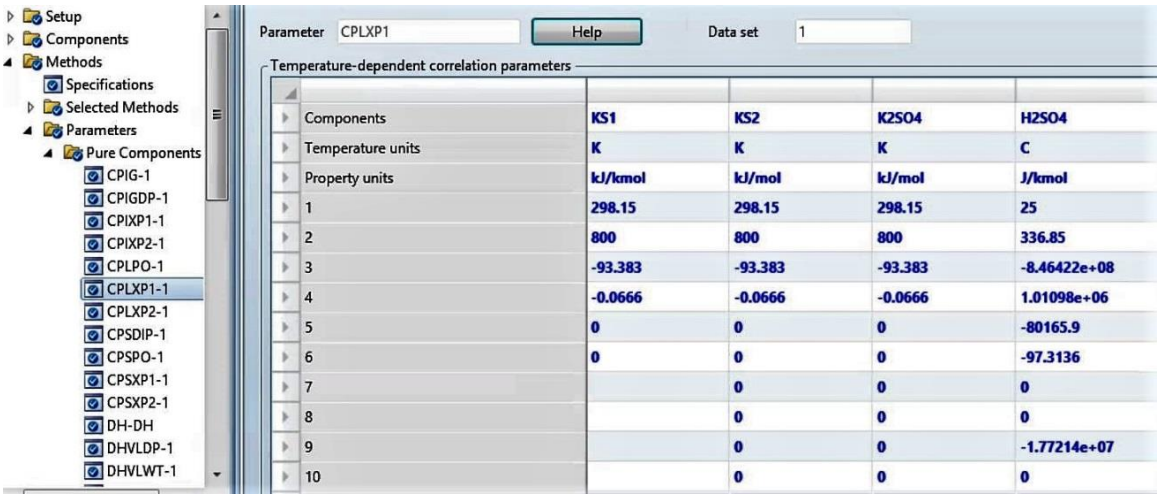

Figure 5: Location and definition of first set data for liquid and solid heat capacity based on Barin model used in flow sheet for component KS1, KS2, and K_2SO_4.

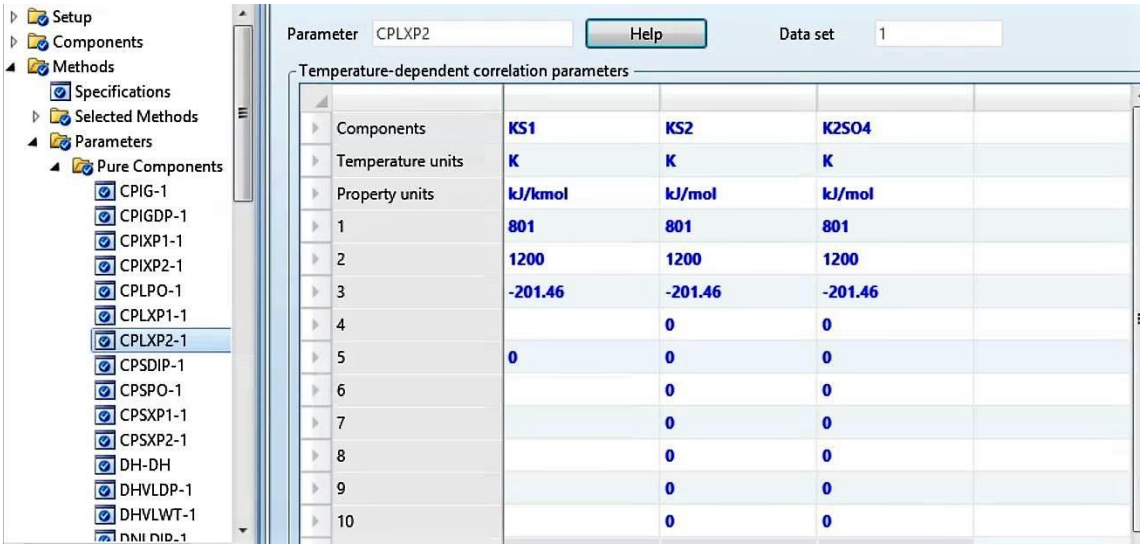

Figure 6: Location and definition of second set data for liquid and solid heat capacity based on Barin model that used in flow sheet for component KS1, KS2, and K_2SO_4.

The polynomial model was chosen i.e. CPLPO for other salts as their heat capacity varies very little over a larger span of temperature. Figure-7 is showing how this heat capacity model was set and what values were used for model parameters

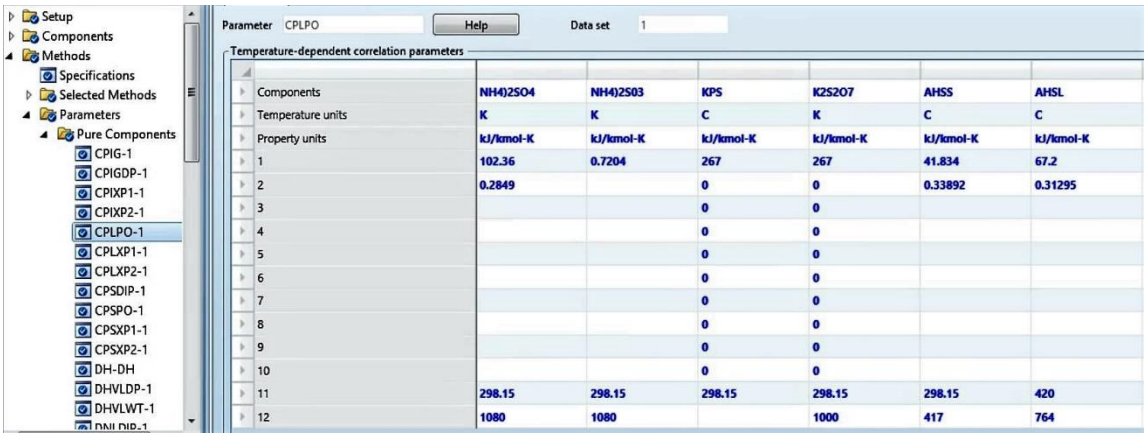

Figure 7: Location and definition of liquid and solid heat capacity for based on a polynomial model that used in the flow sheet for component $(NH_4)_2SO_4$, $(NH_4)_2SO_3$, KPS, $K_2S_2O_7$, AHSS, and AHSL.

The Aspen physical property system has several sub-models for calculating liquid heat capacity. It uses parameter THRSWT/6 to define which sub-model to use. The sub-model we used for different components is shown in Figure 14.

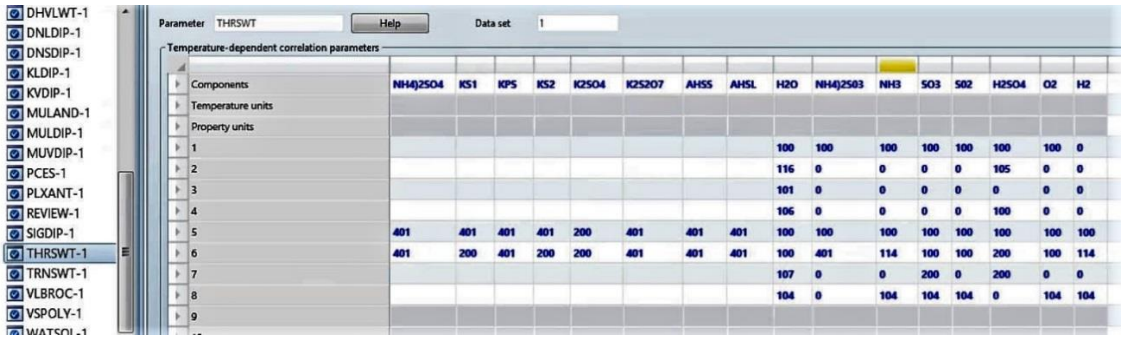

Figure 8: Location and definition of sub-models used in the flow sheet for different components heat capacity.

3.2. AspenPlus model simulation

The Second step for process modeling in Aspen is to prepare the flow sheet. Our developed flow sheet has 25 equipment blocks and a couple of design specification,

calculator, and sensitivity blocks. In the following sections, we will discuss briefly how these blocks were set.

3.2.1. Reactor input and block options

In flow sheet, we used five reactors i.e. LTR, MTR, HTR, Absorber, and Photoreactor. The RStoic model was used for absorber and the photoreactor and RGibbs model for LTR, and HTR. For MTR we choose REquil reactor model as this model is recommended for simultaneous chemical and phase equilibrium calculations. RStoic is selected when the conversion for the reactor is known or can be fixed. If we don't know the conversion, then it is recommended to leave it to thermodynamics to determine chemical, or phase equilibrium i.e. use RGibbs model. Each of these reactors setup and specifications are discussed in the following sections.

3.2.1.3. Absorber

The Rstoic model for the reactor is chosen when the conversion or extent of reaction in the reactor is known. In absorber from literature [34], we know that ammonia is very soluble in water. So we can define conversion of ammonia in the absorber to be 100%. Therefore, we chose RStoic model for the absorber.

In absorber, the operating condition was set as 25°C, and 9 bars with both vapor and liquid was considered as valid phases. The reaction and conversion were specified from absorber setup-reaction tab. Figure-9 is showing how all these conditions and specifications were set up in the absorber.

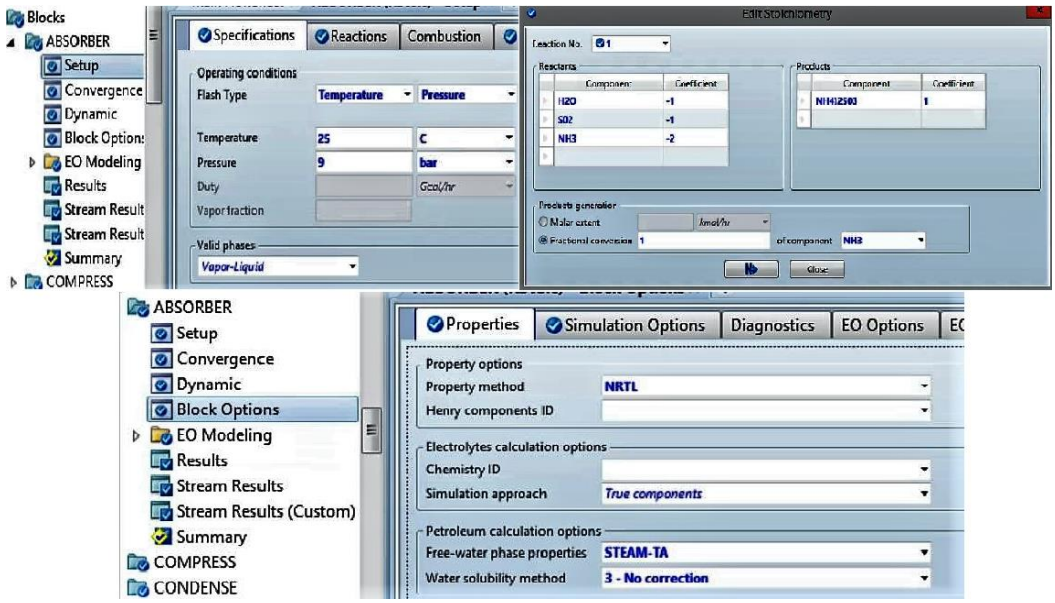

Figure 9: Location and setup for the absorber.

3.2.1.4. Photoreactor

We used RStoic model for photo reactor. We do not know the conversion or extent of reaction in photoreactor, but we know from literature that 25% percentage of photonic energy will convert to hydrogen energy. Therefore, we can correlate this information to determine the reaction conversion. However, for simplicity, we assumed 95% conversion of $(NH4)_2SO_3$ salt for hydrogen formation reaction in the photoreactor.

Again, we performed some sensitivity analysis on the conversion efficiency of solar photonic to hydrogen. For this analysis, we had to vary the reaction conversion, and RStoic reactor model has the provision to vary reaction conversion. it also requires to use design specification block.

The operating conditions were specified from the setup menu where temperature and pressure for the reactor were set as 80°C and 9 bars. Figure-10 is showing, how all these conditions and specifications were set up in the photoreactor.

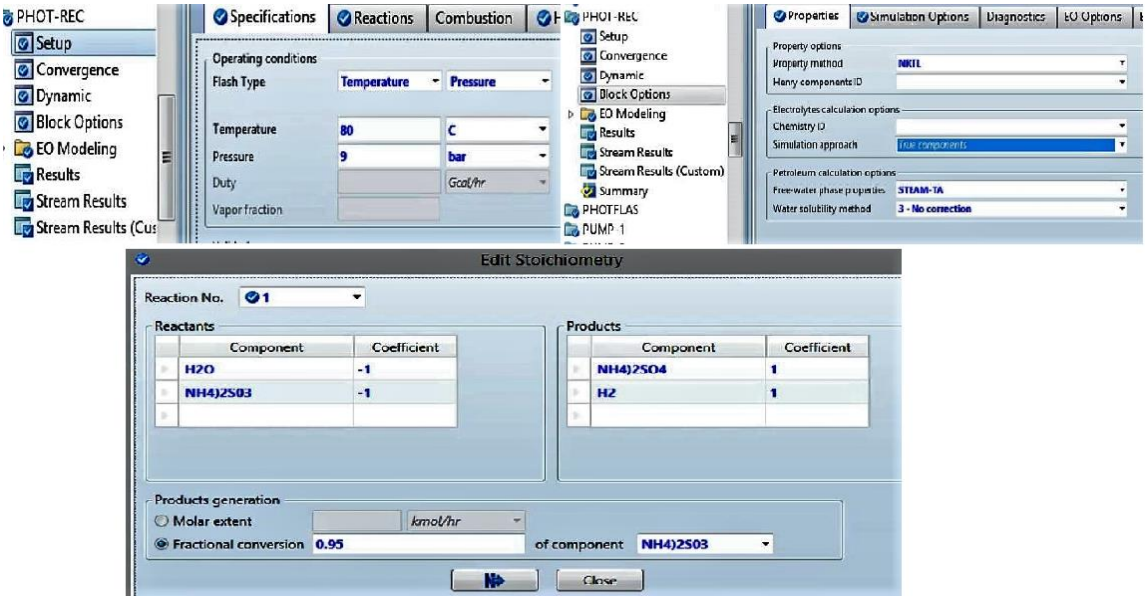

Figure 10: Location and Setup for Photo reactor

3.2.1.5. LTR and HTR

Unlike absorber and photo-reactor, we do not have any information regarding conversion or extent of reaction in LTR and HTR. Thus, RGibbs model was chosen for these two reactors. RGibbs reactor uses Gibbs energy minimization to find the chemical equilibrium in the reactor. RGibbs minimizes Gibbs free energy, subject to atom balance constraints. This model does not require reaction stoichiometry. RGibbs can determine phase equilibrium without chemical reaction, particularly for multiple liquid phases. Any number of liquid phases are allowed we just have to specify reaction conditions.

Figure-11 &-12 is showing, how all these conditions and specifications were set up in LTR and HTR.

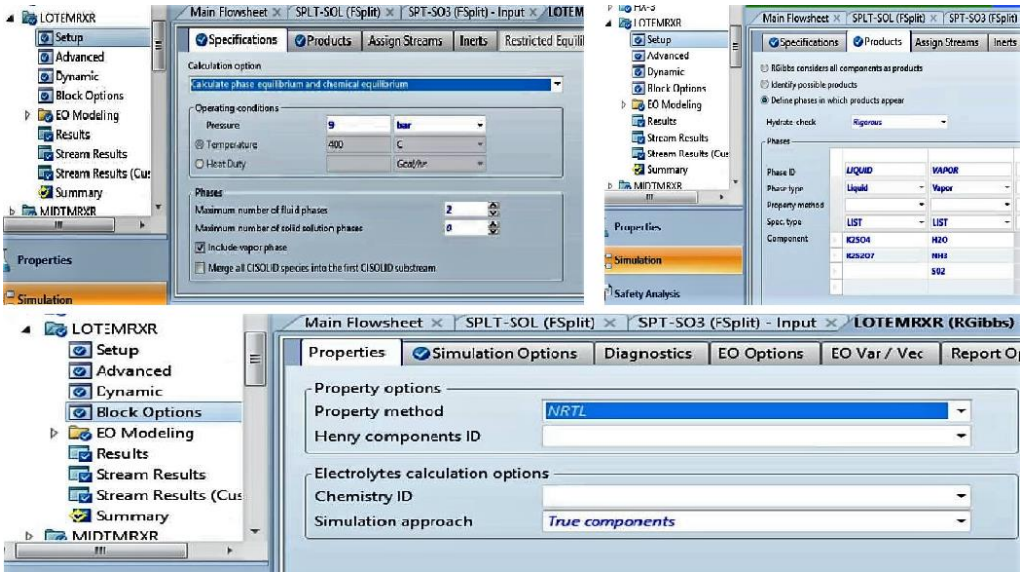

Figure 11: Location of setup and block option of the MTR.

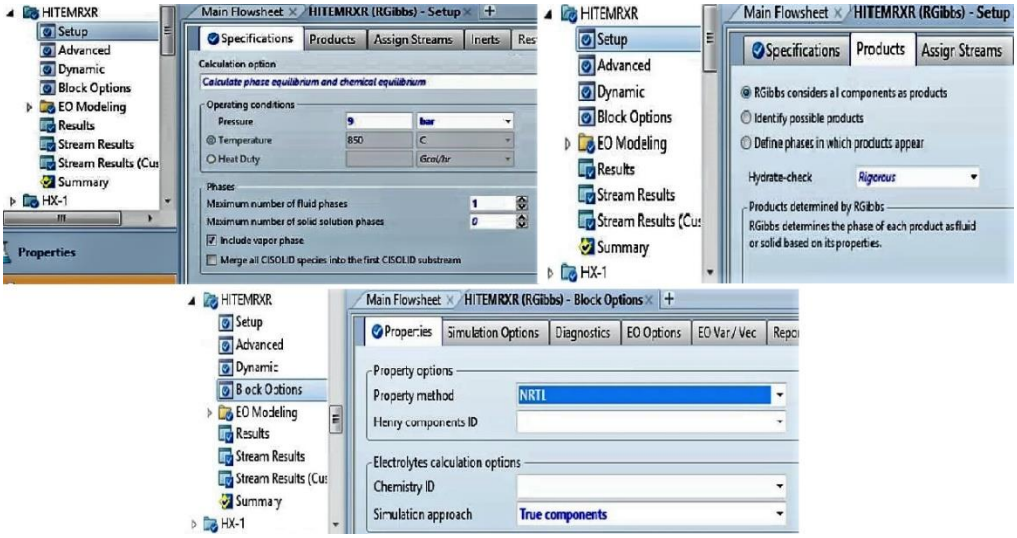

Figure 12: Location of setup and block option of the High-temperature reactor.

3.2.1.6. MTR

In the case of MTR, we used REquil reactor model. REquil models reactors when some or all reactions reach equilibrium. REquil can calculate single phase chemical equilibrium, or simultaneous phase and chemical equilibria. REquil calculates equilibrium by solving stoichiometric chemical and phase equilibrium equations. REquil reactor model is recommended for Vapor Liquid Equilibrium (VLE) and Liquid Liquid Equilibrium (LLE) calculations.

In the MTR we have both LLE and VLE. This is one reason for us to choose REquil model for MTR. Besides that, in this model, we can have reaction extent as one variable. Which is a requirement to force Aspen Plus to follow the Vapor Liquid Equilibrium line in the phase diagram (Figure-2)

How we forced the simulator to follow the VLE line will be discussed in the design specification block section. Figure-13 is showing how we formulated the MTR block in Aspen Plus.

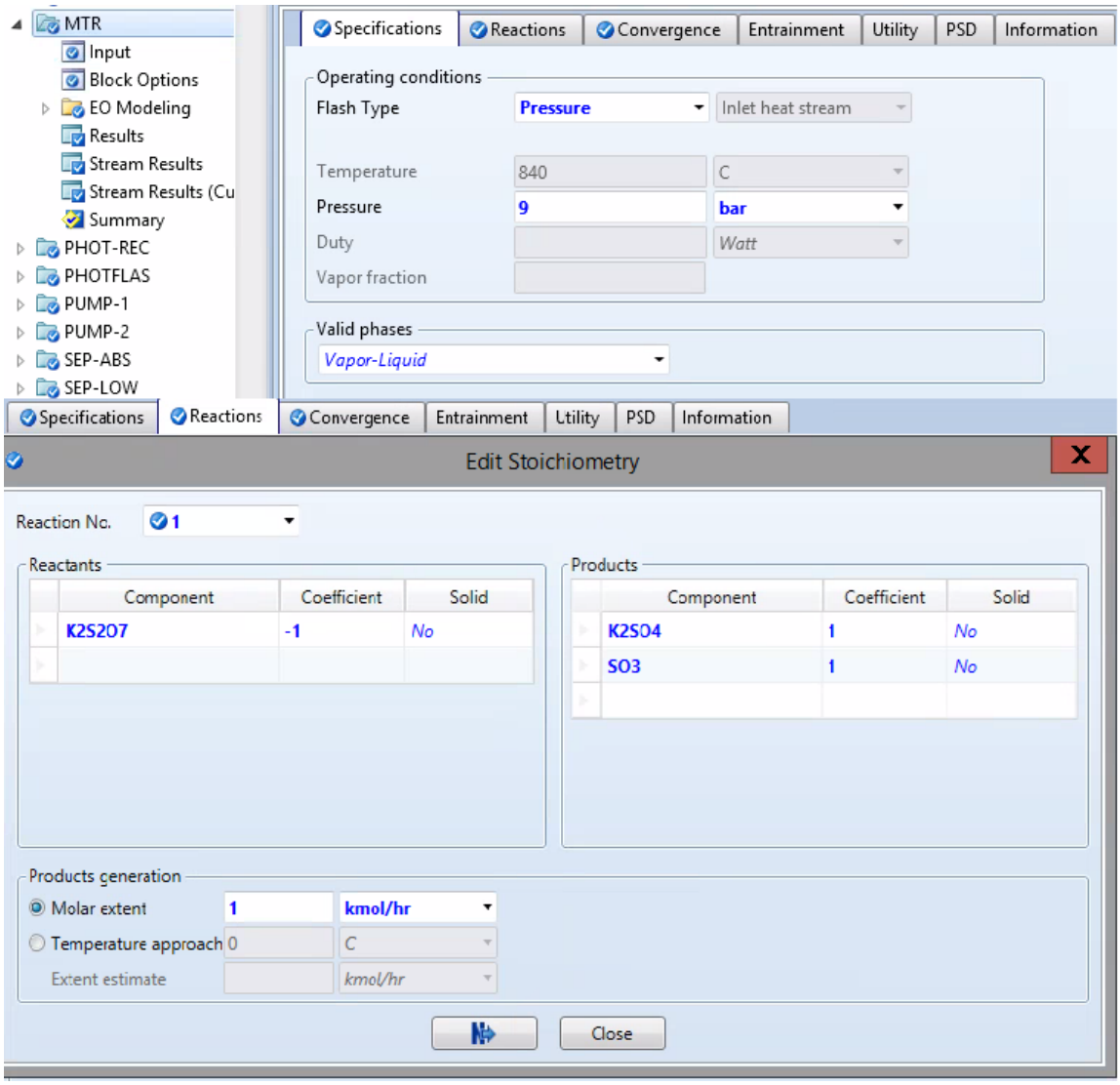

Figure 13: Specifications and setup of MTR

3.2.2. Design specification block

Design speciation blocks are used to manipulate, control or set additional convergence criteria that the simulation will follow. In our model, we used nine design specification blocks in the flowsheet. These are H20-MU, SPHSD-1, SPHSD-2, TC-LTR-1, TC-LTR-2, TC-MTR-1, TC-MTR-2, TC-HTR-1, and TC-HTR-2. The proceeding section will discuss how these blocks were set in detail.

3.2.1.7. H2O-MU block

This design specification block was used to make sure to supply the make-up water required to cover the loss of water from two exit streams. This design specification block was formed by importing two variables from the flow sheet i.e. water flow rate in the recycled ammonium salt-stream and water flow rate in the feed ammonia salt. These two variables were named WH201 and WH202 consecutively. In this design specification block, the mole flow rate of feed water was varied to make WH201 and WH202 equal. Figure-14 is showing how variables and conditions are defined and varied to meet the condition.

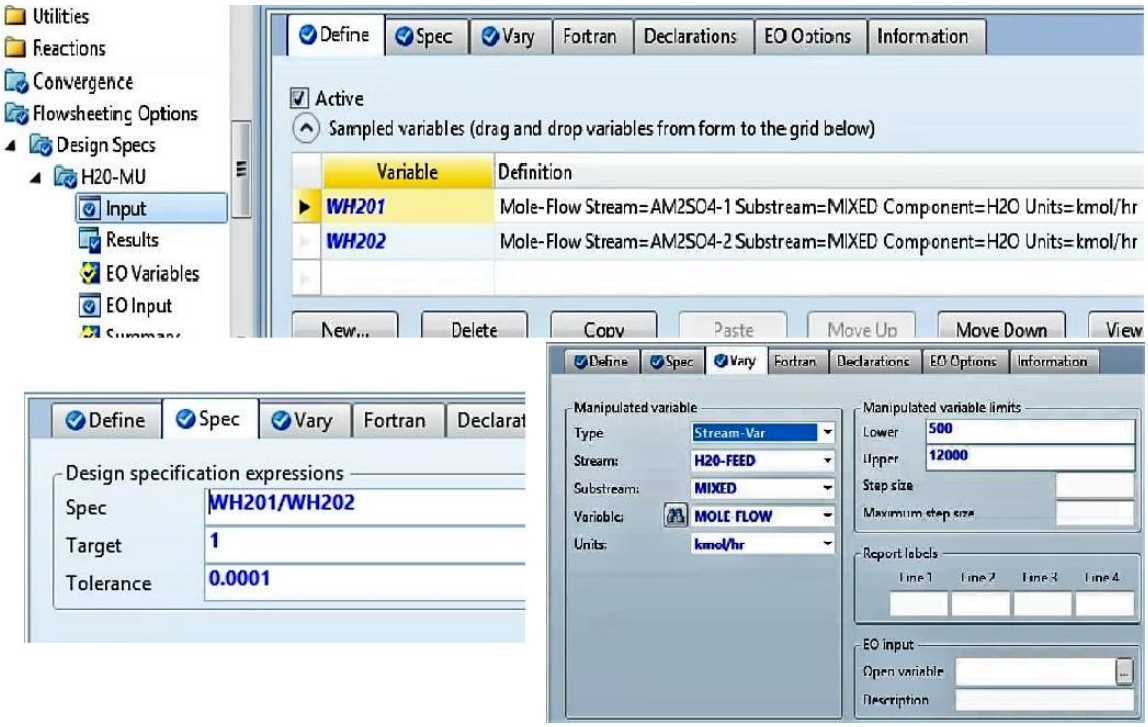

Figure 14: Steps involved in defining MU-H2O design specification block

3.2.1.8. SPHSD-1

We used the SPHSD-1 design specification block to make sure that the composition of K_2SO_4 stays on the line-1 in the salt phase diagram (Figure-2). From the Excel plot, we find out that the equation for this line is

$$T = 1308.9 \times (XK_2SO_4)^{0.2414}$$

Where,

XK_2SO_4 = Mole fraction of K_2SO_4 salt in solution.

T = Temperature of the feed stream.

The temperature of the feed stream is the same as the LTR, so the equilibrium composition of the stream will not change from the point of feed to LTR.

In this design specification block, we varied the mole flow rate of K_2SO_4 against a fixed flow rate of $K_2S_2O_7$ to find the flow rate of K_2SO_4 which can absorb all the released NH_3 from Ammonium sulfate salt. This design specification block checks for each feed composition whether it is following the equilibrium line's equation or not. The block will only converge when it finds a point that is on the line. Figure-15 is showing how we setup this block in Aspen Plus.

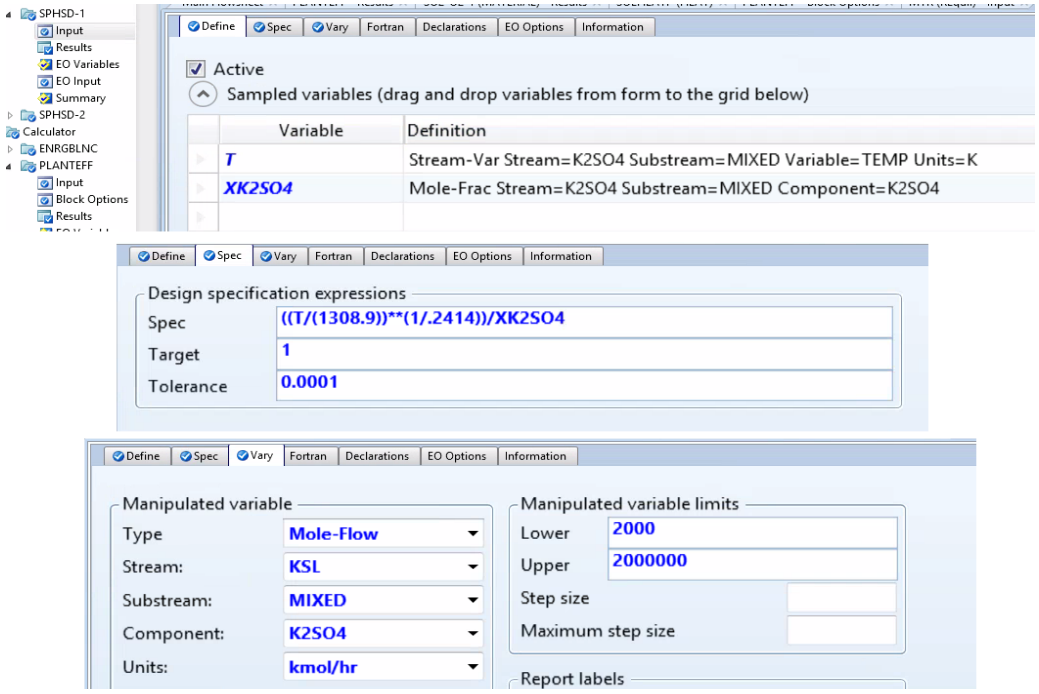

Figure 15: Location and setup of design specification block SPHSD-1.

3.2.1.9. SPHSD-2

We used SPHSD-2 design specification block to determine the conversion in MTR. Similar to the SPHSD-1 design specification block we used the digitized equation of the line-3 of the phase diagram (Figure-2) in the following form to set the mathematical constraint in determining the extent of reaction in MTR.

$$\left[10^{\{-9.94+22.6*\frac{T}{1000}-(13.53*\frac{T}{1000})^{0.838}\}}\right]-\left(\frac{P\times XK_2SO_4}{1-XK_2SO_4}\right)=0$$

Where

XK_2SO_4 = Mole fraction of K_2SO_4 salt in solution.

T = Temperature of the feed stream.

P = Pressure of MTR

Figure-16 is showing the setup and specification of this SPHSD-2 block

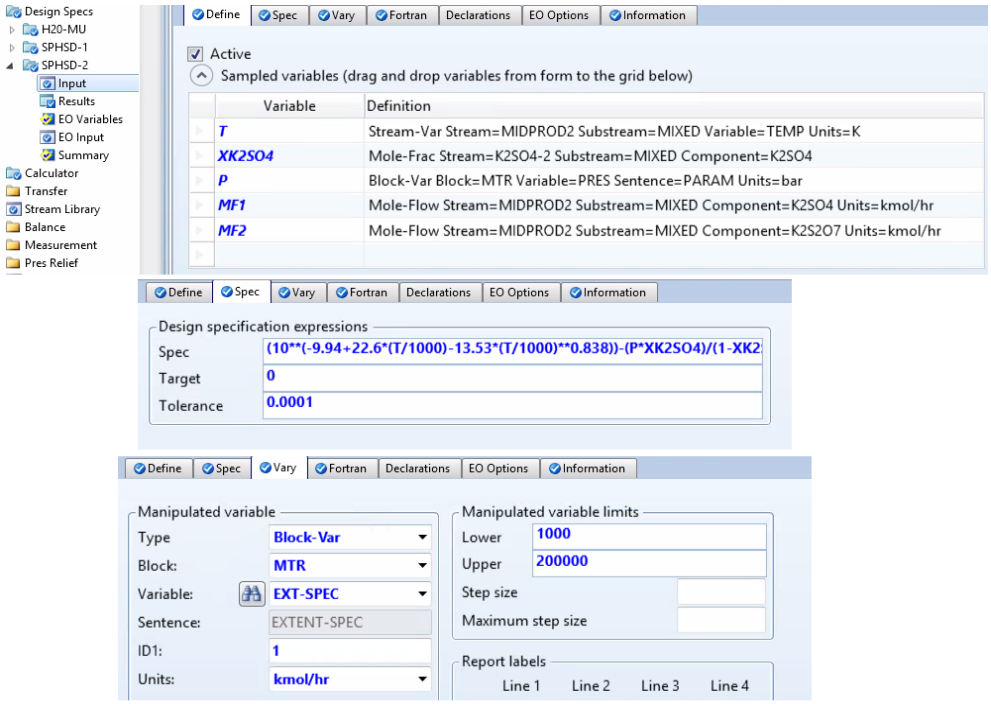

Figure 16: Location and setup of design specification block SPHSD-2

3.2.1.10. Temperature controller (TC)

These design specification blocks were devised to integrate the thermal energy storage system into the flow sheet. In the process flow sheet, six temperature controllers were used to maintain three reactors temperature i.e. LTR, MTR, and HTR.

Each reactor has two TC and two different temperature streams connected to it except HTR. For HTR only one TC is attached to it. The TC will increase the flow rate of cold or hot salt or gas stream to keep reactor temperature near set temperature.

Each controller imports two variables from the flow sheet i.e. the hot or cold streams flow rate and the concern reactor's temperature. Then compares the imported reactor's temperature with the set point and the design specification block tries to keep the difference between the two temperatures at zero by increasing gas or salt flow rate.

For example, in the case of LTR, if the reactor receives less solar heat energy than required, its temperature will decrease. In such situation, the TC-LTR-1 design specification block will increase the hot salt's flow rate until the difference of imported and set temperature becomes zero. An error tolerance of 0.0001 for the temperature difference was set. Figure-17 is showing how one such temperature controller was defined in Aspen Plus.

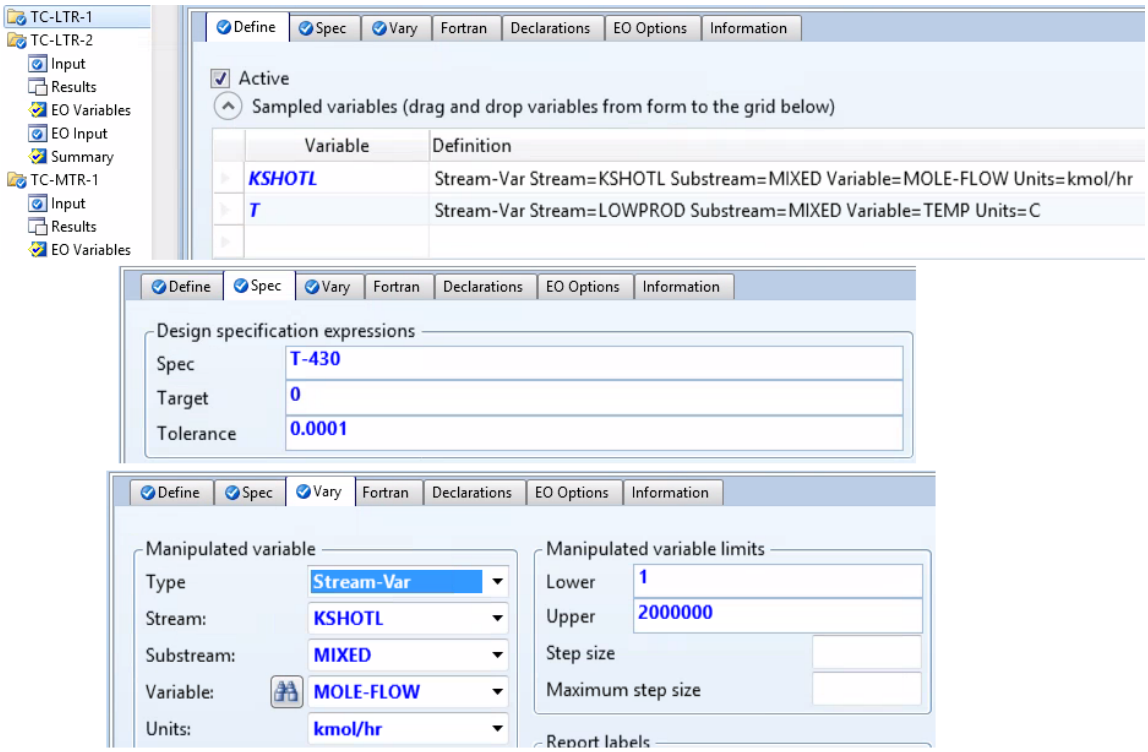

Figure 17: Steps involved in defining the TC-LTR-1 design specification block

3.2.3. Calculator block

Calculator blocks help to write additional equations for the simulation. These additional equations can be used to calculate certain properties and parameters. The calculator block is equipped with a FORTRAN window to write equations for calculating the value of the required parameters or terms.

Calculator blocks are designed by first defining pertinent variables associated with the concerned value and their information (either imported or exported). Then in the FORTRAN window, all the equation to calculate the concerned values are written. The calculated value can be exported to use where it is needed in the flow sheet, or it can be displayed as a standalone value for reference to the designer.

In the process flow sheet, we used two calculator block one is to calculate the efficiency of the process and the second to calculate what percentage of total energy is photonic energy. These blocks are described in detail in the following two sections.

3.2.1.11. Efficiency block (PLANTEFF)

To calculate efficiency following equations based on literature [35] were used

$$\text{Efficiency} = \frac{\text{Lower heating value of Hydrogen produce}}{\text{Net energy consumption}} \tag{40}$$

$$\text{Lower heating value of Hydrogen} = 67177.6 \times \text{Flow rate of produced Hydrogen} \tag{41}$$

$$\text{Net energy consumption} = \text{Total energy consumption} + \text{Total work produced} \tag{42}$$

To include Eq.(40) in Aspen Plus, nine variables were imported from the flow sheet. Then all these equations were written in the FORTRAN window of the calculator block. Figure 18 is showing the names of all the imported variables and different steps involved in defining this block.

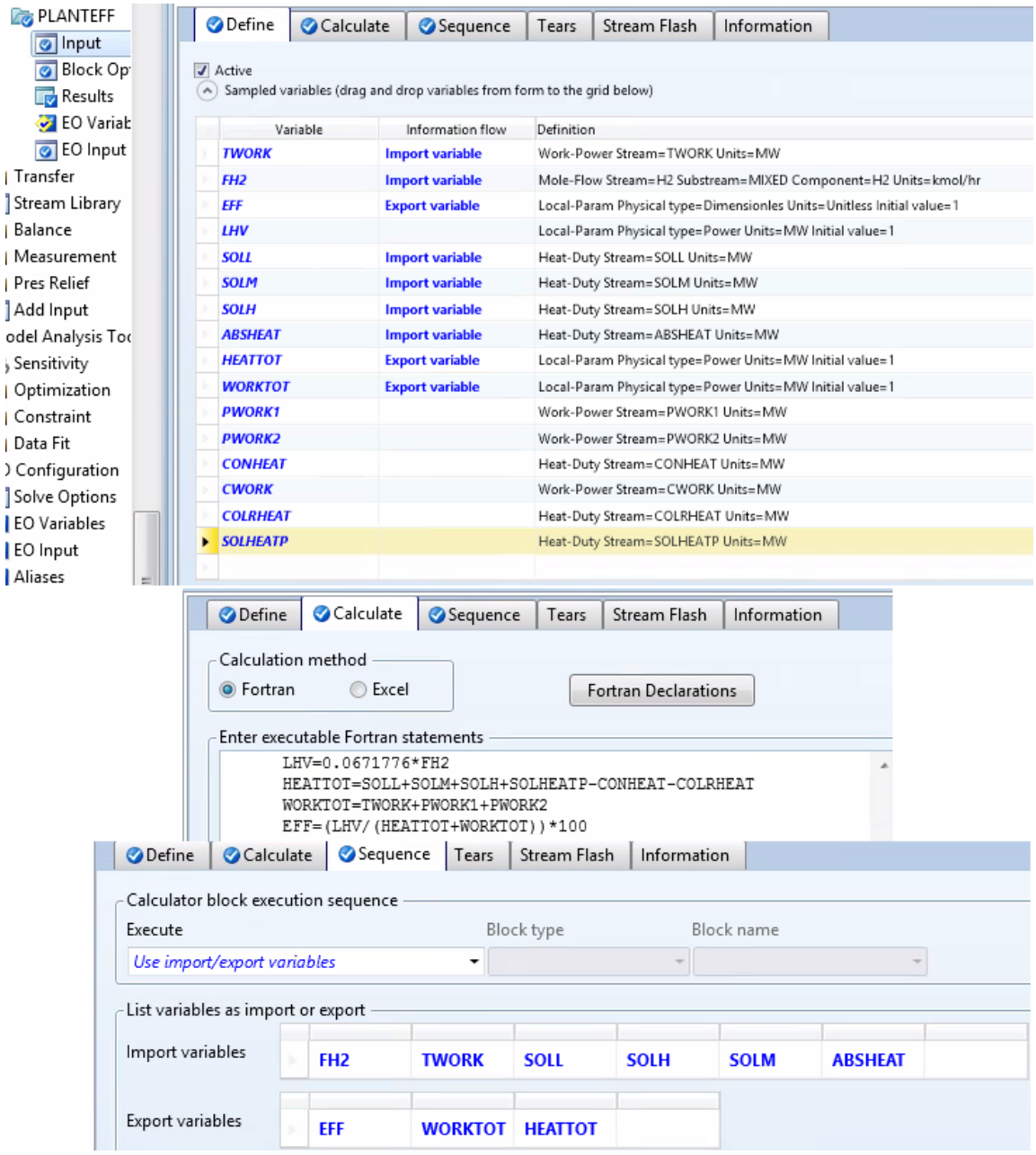

Figure 18: Steps involved in defining the PLANTEFF calculator block.

3.2.1.12. Energy balance (ENRGBLNC)

The purpose of this block is to calculate the percentage of the thermal and photonic energy in total consumed energy. For this energy balance block, four variables were imported from the flow sheet, and following equation was used in FORTRAN.

$$\text{Percentage of Photonic energy} = \frac{\text{Photonic energy}}{\text{Total Energy}} \times 100 \tag{43}$$

From literature [34], we know that 19% of solar energy is photonic energy. This block will indicate whether the process is following this convention or not. Figure-19 is showing how this block was defined in Aspen Plus.

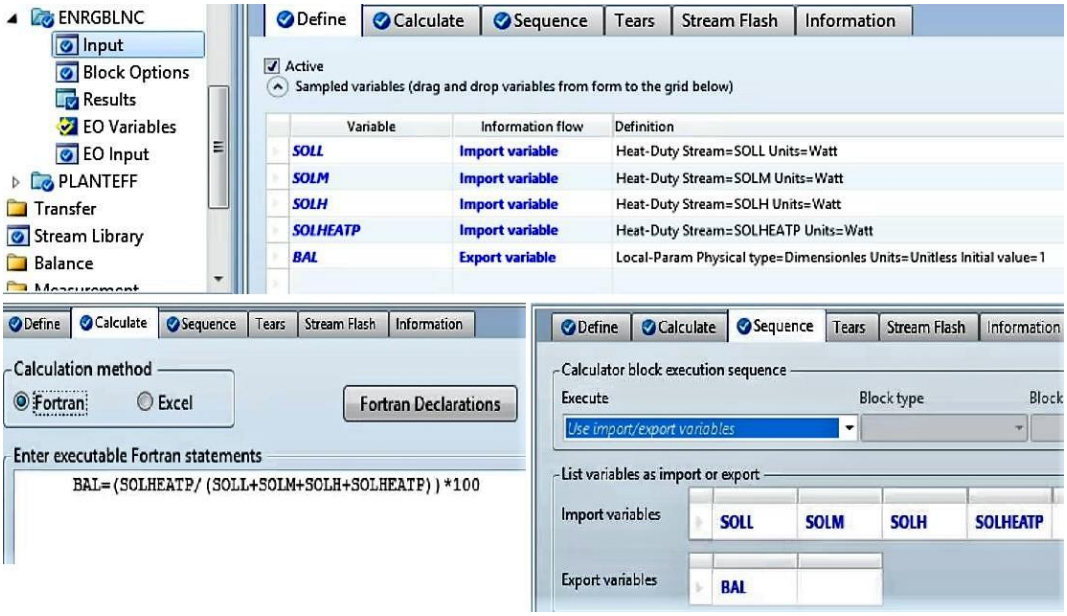

Figure 19: Steps involved in defining the ENRGBLNC calculator block.

3.2.4. Sensitivity block

The sensitivity block can be used to find out the dependence of one variable on one or more variables. It helps the process designer to find how sensitive key parameters are to variations of other parameters or disturbance.

Defining of sensitivity block is like a calculator, and design specification blocks start with defining pertinent variables. Then the independent variable is defined by defining its lower and upper limit and certain interval or number of points within the limit. Then variables are selected to form the data table. Then this table can be used to plot mutual relationship of different variables.

In developed flow sheet, we used one sensitivity block to evaluate the sensitivity of process efficiency to feed composition and three reactors temperature. This sensitivity block is discussed in detail in the following section.

3.2.1.13. FC-RT

FC-RT sensitivity block was used to see the sensitivity of efficiency to the mole fraction of potassium pyrosulfate and reactor temperatures.

First, all the pertinent variables were defined. These include all the variables required to calculate efficiency and the variables whose effect on efficiency we want to investigate. The second group includes mole fraction (FACKPS), three reactor's temperature. (TL, TM, TH). The naming of all these variables was required so that we could collect data and put these data in a table.

In the 'vary' section of the sensitivity block, all three reactors temperature and feed flow rate of potassium pyrosulfate were defined and assigned range, for variation

with an interval of change. Feed flow rate manipulation results in potassium sulfate's composition to vary from 0.053 to 0.086. The temperatures were varied with an interval of 20°C from 410°C to 500°C, 800°C to 890°C, and 800°C to 950°C for LTR, MTR, and HTR consecutively. For HTR the interval was 5°C.

A FORTRAN code was written to calculate the efficiency as we wrote in calculator block.

We can run this sensitivity block with any combination of the four manipulated variables making one or more active or deactivate. However, some changes in flow sheet are required.

For example, if we want to run the sensitivity of temperature then we should make temperature as an independent variable in reactors i.e. instead of connecting the heat duty stream as input we need to connect those as an output from the reactors. In addition, we need to re-identify the three solar heat streams and reverse their sing in the FORTRAN code for efficiency calculation. In addition, we have to tabulate the manipulated variables accordingly. Figure-20 is showing how this sensitivity block was set up in Aspen Plus.

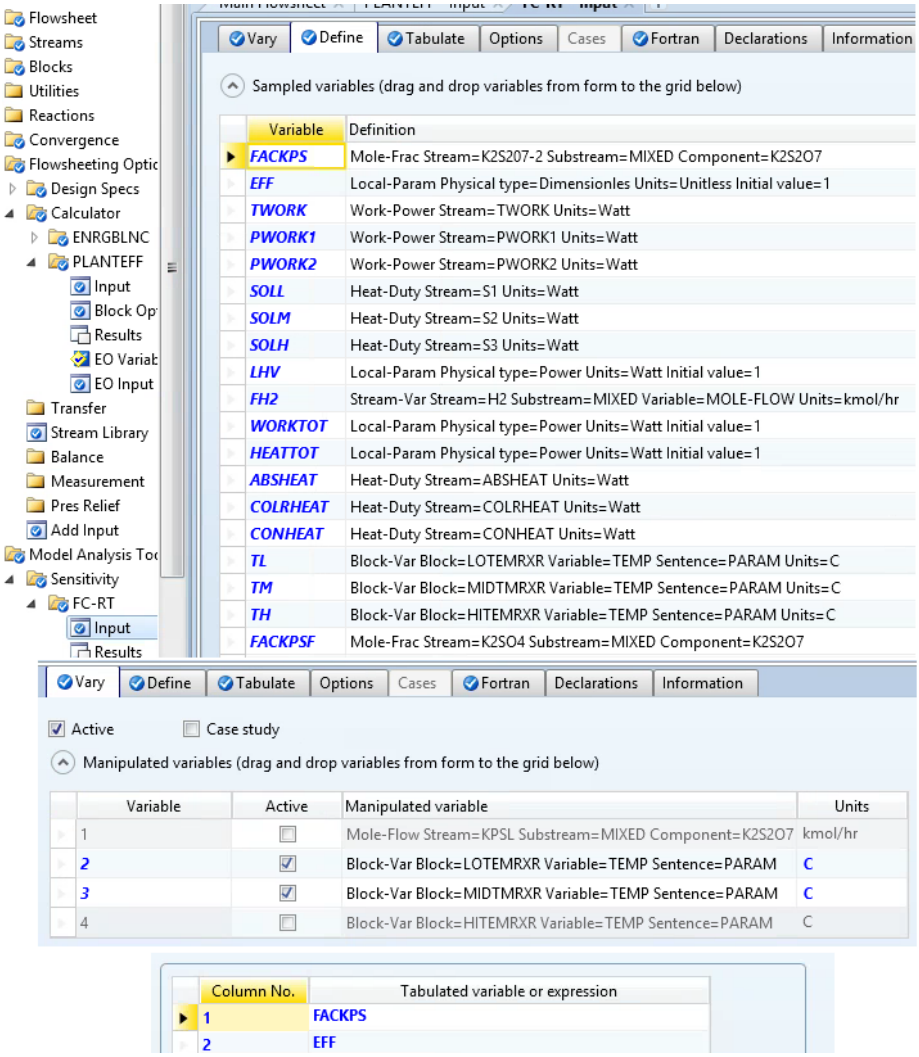

Figure 20: Defining of sensitivity block FC-RT.

3.2.5. Economic analysis

Aspen Plus process simulator has built in economic analysis tools to calculate the capital cost, installation cost, operation cost and another associated cost for the preliminary economic analysis of different scenarios. We communicated with few supplier and based on their quotation we specified a price for different input and output streams.

Then when we ran the economic analyzer module in Aspen Plus, it calculated all associated costs and investment required to build and operate the plant. Then we used this data in calculating the Internal Rate of Return (IRR) and Minimum Acceptable Rate of Return (MARR) [36]for evaluating the economic feasibility of both options of the hydrogen production process i.e. process with TES and process without TES.

4. ERROR AND WARNING ANALYSIS

Once simulation of the prepared flow sheet converged, the overall result of the simulation can be seen from the control panel. The control panel reports three types of error, and these are property error, system error, and simulation error. It can also report if there are any warnings. The flowsheet we prepared based on the methodology described in Chapter 3, showed only one simulation error and no property or system error. Figure 21 is showing the error list from the control panel.

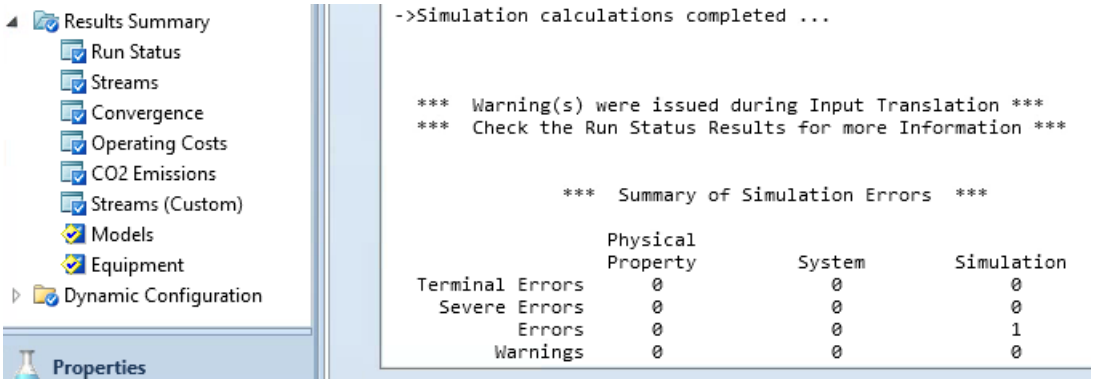

Figure 21: Summary of simulation errors in Aspen Plus 8.8 control panel.

This simulation error results when Aspen began the calculation for the convergence loop $OLVER 02. This error stated that at the beginning of the simulation since there is zero feed to the heat exchanger, HX-3 the sum of duty of heat streams is zero. And to continue calculation Aspen bypassed calculation of this block at the beginning of the calculation. Figure 22 is showing the snapshot of the part of control panel containing this error.

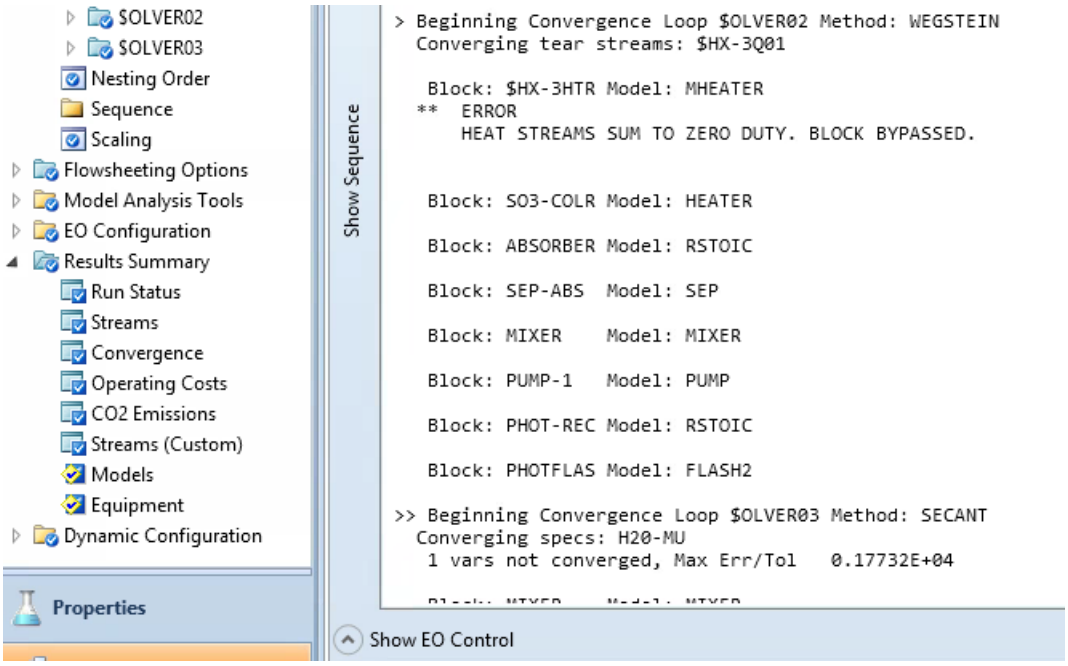

Figure 22: Location and detail of the simulation error in the control panel of the Aspen Plus simulator.

But eventually, when Aspen finished calculation of other convergence loops, it performed the calculation of this bypassed block. Figure 23 is showing that Aspen finished the calculation of this block when all the other convergence loop were converged.

```
>> Loop $OLVER03 Method: SECANT       Iteration    1
  Converging specs: H20-MU
# Converged              Max Err/Tol   0.19854E-01

   Block: $HX-3H01 Model: HEATER

> Loop $OLVER02 Method: WEGSTEIN     Iteration    2
  Converging tear streams: $HX-3Q01
# Converged              Max Err/Tol   0.41204E-09

   Block: H2SEP    Model: SEP

   Block: COMPRESS Model: COMPR

   Calculator Block PLANTEFF

->Generating block results ...

    Block: PUMP-1   Model: PUMP

    Block: PUMP-2   Model: PUMP

    Block: $HX-1HTR Model: MHEATER

    Block: $HX-2HTR Model: MHEATER

    Block: $HX-3HTR Model: MHEATER

->Simulation calculations completed ...
```

Figure 23: Snapshot of part of control panel where the bypassed block were solved.

5. RESULTS AND DISCUSSION

In this study, we tried to meet the prime objectives discussed in Chapter 2. Besides these objectives, we also run some analysis of the developed process to check its sensitivity and dependence on some key parameters. We will describe and discuss all these results in the preceding sections.

5.1. Process flowsheet

Aspen Plus process simulator was used to design this process flowsheet. Figure-28 is showing the process flowsheet developed in this work for the hydrogen production process based on HySA cycle. Development of this process flow sheet was challenging because of associated convergence issues. Aspen uses sequential modular method for converging a flow sheet. The sequential modular method of solving the system of equations associated with the flow sheet means that if there is an issue in one block, it will result in an error in converging the entire process. This made the task of converging all the equipment blocks together difficult. Therefore, we converged the flow sheet block by block.

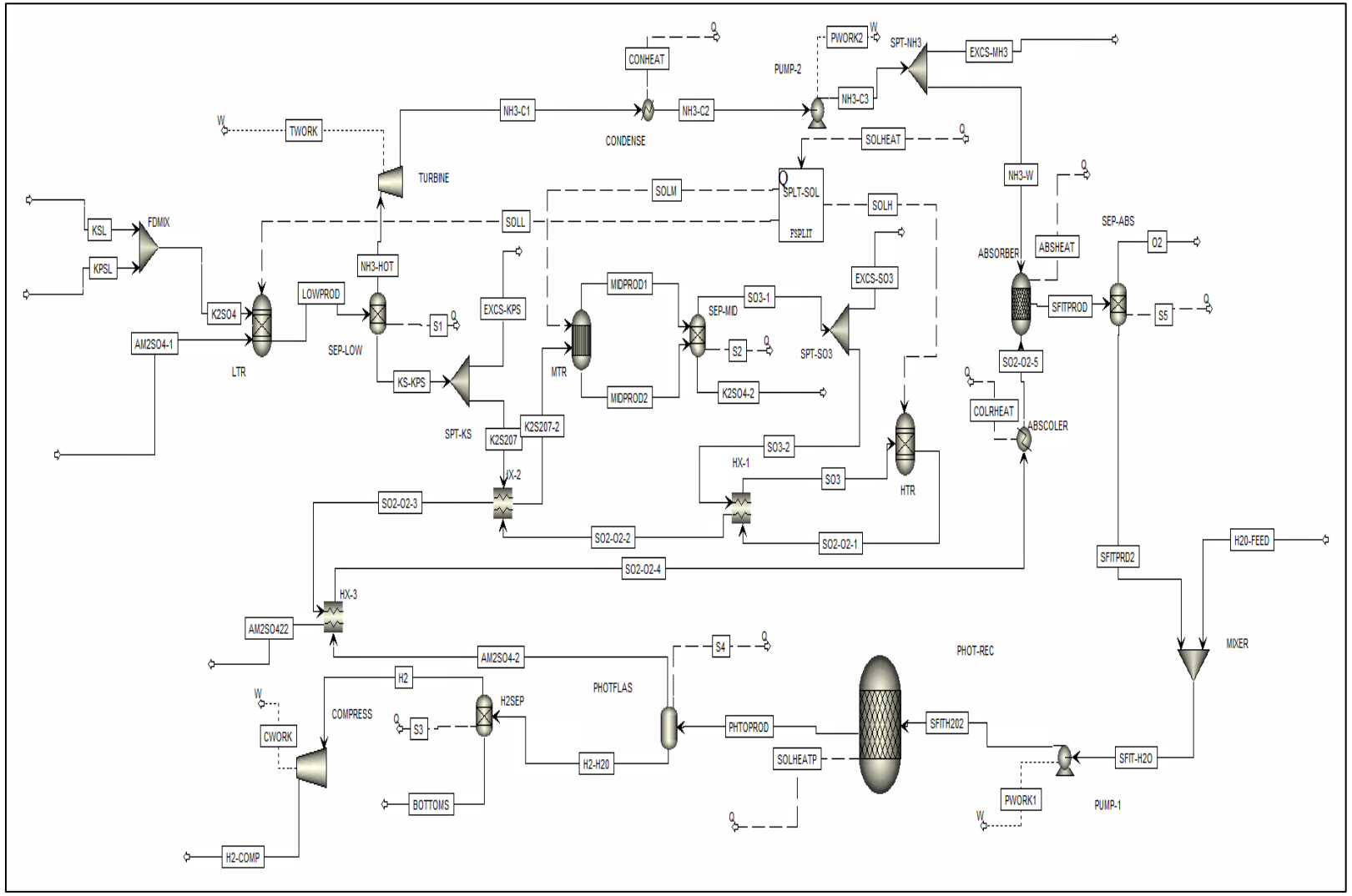

Figure 24: Process flow sheet of the developed photo-thermo-chemical hybrid sulfur-ammonia hydrogen production plan in the current work

To aid the convergence, we followed the methodology discussed in Chapter 3 i.e. reactor specification, design specification, manual input of thermodynamic properties, thermodynamic model, and manual tear stream. In the following sections, we will discuss some steady state simulation results without thermal energy storage system.

5.1.1. Material and energy balance sheet

The material and energy balance data sheet for the entire flowsheet will be displayed in tables in Appendixes. However, Table 1 & 2 is showing the material and energy balance in summary for the entire flowsheet. The design basis for all steady-state calculation of the flow sheet was 7004 kmol/hr. hydrogen (14120 kg/day hydrogen for 12-hrs. /day operation).

Mass flow in [Kg/Kg of H2]			**Mass flow out [Kg/Kg of H2]**	
Main Feed			**Main Output**	
Feed Water	8.96		Hydrogen product	1
			Oxygen Product	7.94
			Liquid from hydrogen separator	1.995
Recycle stream Supply			**Recycle stream Return**	
Ammonium sulfate	115		Ammonium sulfate	115
Potassium sulfate	4757.7		Potassium sulfate	4757.7
Total	**4881.76**		**Total**	**4881.73**
Difference				**0**

Table 1: Summary mass balance for the process flowsheet.

Energy in (KW per Kmol/Hr H2)			Energy out (KW per Kmol/Hr H2)	
Low-temperature reactor	140.08		Ammonia Condenser	59.02
Mid-temperature reactor	151.88		Absorber	151.62
High-temperature reactor	28.05		Oxygen product	0
Photo reactor duty	49.68		Hydrogen product	68.26
Potassium sulfate feed	20682.02		Ammonium sulfate return	579.66
Ammonium sulfate feed	576.52		Potassium sulfate return	20657.47
Feed water	0		Low-temperature reactor product separator	0.02
Ammonia Pump	0.02		Mid-temperature reactor product separator	4.17
Water pump	0.02		Absorber product separator	0.0
Hydrogen product Compressor	1.08		Photo reactor product separator	5.91
			Hydrogen separator	0.04
			Bottom product from Hydrogen separator	0.25
			Absorber pre-cooler duty	32.86
			Turbine power generation	14.76
			Heat loss from system	55.25
Total	21629.35		Total	21629.29
Difference				0.0

Table 2: Summary of energy balance for the process flowsheet.

From literature [35], we know that 81% of solar energy is thermal and 19% is photonic. From this table, we calculated that photo reactor utilized 14% of the total absorbed solar energy. Therefore, we can conclude that the process is consuming less

photonic energy than the allowable ratio. However, a calculator block; ENRGBLNC, was used in the flowsheet to report this ratio.

The heat duty of absorber pre-cooler and absorber includes cooling the two feed stream i.e. NH3-W and SO2-O2-4 to the operating temperature (25°C) of the absorber and released heat from the absorption reactions.

The separator heat duty includes released heat from five separators i.e. product separator of the LTR, MTR, Absorber, Photo reactor and hydrogen separator. The released heat from LTR and Absorber separator are negligible i.e. close to zero.

5.1.2. ENRGBLNC

We have already discussed the methodology and setup of this calculator block. In section 3.2.3.2. Table 3 is showing the result of this block. This block always reports the percentage of photo energy in absorbed solar energy using Eq. (43)

Variable	Value	Units
Solar thermal energy consumed by the Low-temperature reactor (SOLL)	981.11	MW
Solar thermal energy consumed by the Mid-temperature reactor (SOLM)	1063.76	MW
Solar thermal energy consumed by the High-temperature reactor (SOLH)	196.49	MW
Photo reactor energy consumption (SOLHEATP)	348.04	MW
$BAL=\frac{SOLHEATP}{SOLL+SOLM+SOLH+SOLHEATP}\times 100$		
$=13.43\%$		

Table 3: Results of ENRGBLNC calculator block indicating the indicating the proportion of solar thermal to solar photo energy.

From literature, we know that the solar concentrator can convert 50% of total available thermal energy in solar radiation. This available thermal energy is 81% of total energy. Rest of 19% is photonic energy, and available photo reactor can convert 25% of this energy to hydrogen energy.

After including these conversion efficiencies, we found that the percentage of photonic energy should be 23.7% of total solar energy. This is not following the ration of solar photonic and thermal part. Therefore, we need either to recalculate the initial reflector's diameter or to use more efficient photo reactor. We started our calculation with reflector diameter of 1.784 km, but if we want to meet, this constraint of solar photonic and thermal ratio then we need a reflector disk of 3.588 km diameter. Then the solar thermal energy will be more than required, and a substantial amount of it must be wasted by defocusing the reflector. Around 55.85% of the thermal energy must be wasted by defocusing the reflector at steady state plant operation.

5.1.3. Flowsheet efficiency

The process simulation was executed at steady state conditions, i.e. constant input of solar energy and feed material. The overall efficiency was calculated based on Eq. (40), (41) and (42)

A calculator block named PLANTEFF, as described in the section-3.2.3.1 was used in Aspen Plus to calculate the efficiency of the flow sheet. An overall solar to hydrogen efficiency without considering the solar concentrator and photo reactor's efficiency is found to be 25.57%. in this calculation we did not consider the released energy from absorber as useful energy. This is because absorber operates at 25˚C. However if we

consider released energy from absorption reaction useful energy like the previous attempt [13], then the calculated efficiency will be 50%. Table 4 is showing results of PLANTEFF block in detail.

Variables	Value	Units
Work generated from turbine (TWORK)	103.38	MW
H2 product flow rate (FH2)	7004.17	kmol/hr
Lower heating value of hydrogen (LHV)	470.5	MW
Solar thermal energy consumed by the Low-temperature reactor (SOLL)	981.11	MW
Solar thermal energy consumed by the Mid-temperature reactor (SOLM)	1063.76	MW
Solar thermal energy consumed by the High-temperature reactor (SOLH)	196.489	MW
Solar photonic energy required in photo reactor (SOLHEATP)	347.82	MW
Heat recovered from ammonia condenser (CONHEAT)	413.39	MW
Heat recovered from absorber pre-cooler (COLRHEAT)	230.19	MW
Energy released by Absorber (ABSHEAT)	1178.32	MW
Work required for the liquid ammonia pump (PWORK1)	0.15	MW
Work required for the water pump (PWORK2)	0.21	MW
Efficiency, $EFF=\frac{LHV}{((SOLL+SOLM+SOLH+SOLHEATP-CONHEAT-COLRHEAT)+(TWORK-PWORK1-PWORK2))}\times 100$ =25.54 % (50%)		

Table 4: Results of the PLANTEFF calculator block

This calculated efficiency did not take into account the efficiency of the solar concentrator. This efficiency should be multiplied by the solar concentrator's efficiency to report the complete efficiency of the process including a solar concentrator. If we

consider the solar concentrator's efficiency and the efficiency of photo reactor as discussed in section 5.1.2, then this calculated solar to hydrogen efficiency will reduce to 12.55%.

5.1.4. Sensitivity of efficiency

In the flowsheet, we tested the sensitivity of efficiency on feed composition and reactor temperature. For this sensitivity analysis, FC-RT sensitivity block was used as described in section -3.2.4.1. This sensitivity block was set in such a way that we could run it in several different modes or combinations of variables. This sensitivity analysis helped us to determine the optimum operating condition for reactors and feed composition. All these different modes are discussed in the following sub-sections.

5.1.4.1. Mode-1

In mode-1, we explored the sensitivity of efficiency on feed composition. We ran the sensitivity block for six different operating temperatures of the MTR. We then used the results of this block to plot the graph shown in Figure-25.

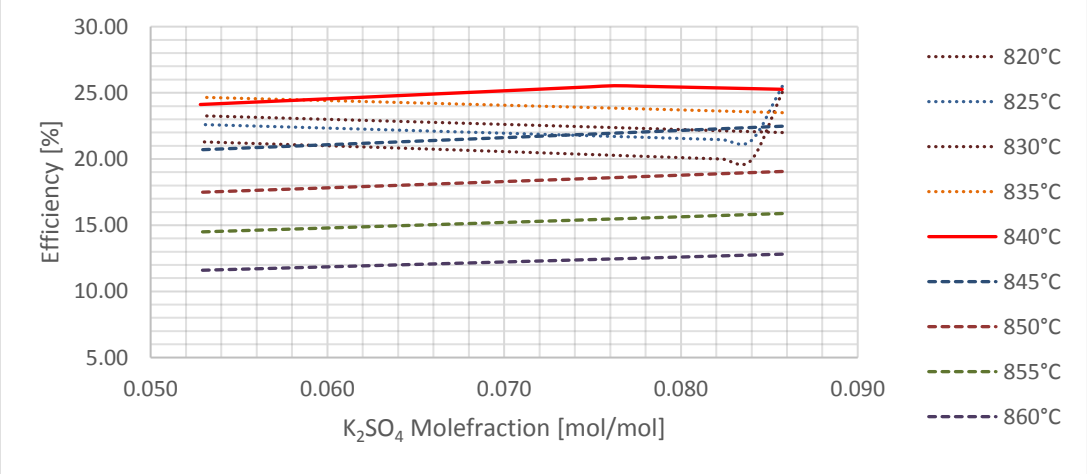

Figure 25: Sensitivity of efficiency on feed potassium composition at six different MTR temperature.

From this plot, we can conclude that the maximum efficiency point resulted at 840°C of MTR and 0.076 mole fraction of K_2SO_4. The point of maximum efficiency decreases if we increase the percentage of K_2SO_4. This decrease in maximum efficiency resulted because; as we increased the mole fraction of K_2SO_4 beyond 0.076 the process was stepping into the solid region of the phase diagram (Figure-2).

5.1.4.2. Mode-2

In mode-2, we investigated the sensitivity of efficiency on the temperature of LTR, MTR's temperature. Figure-26 is showing a 3D MATLAB contour plot of results of the FC-RT sensitivity block. During this mode, feed composition and HTR's temperature was kept constant.

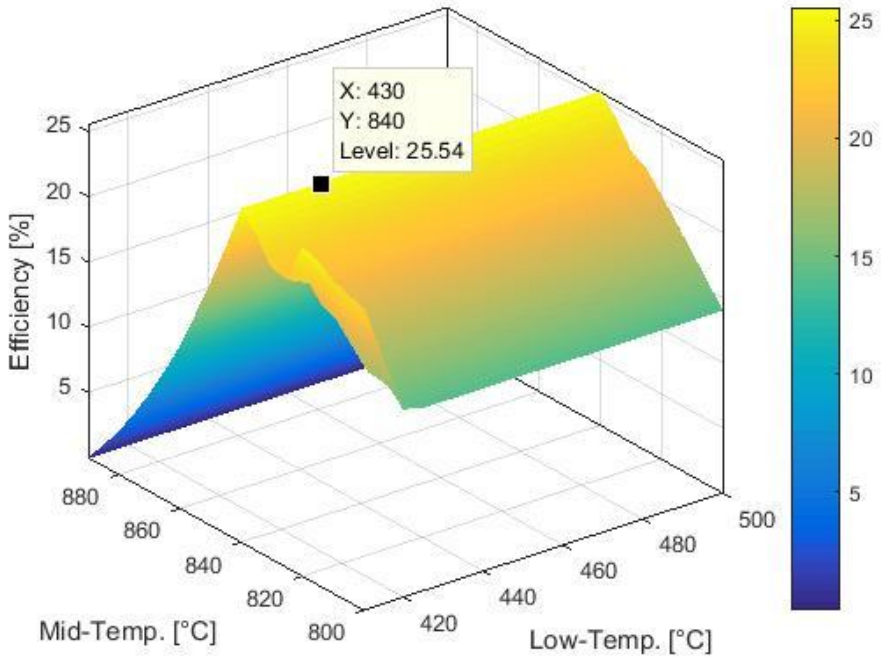

Figure 26: Sensitivity of efficiency on operating temperature of both LTR and MTR.

From this contour plot, we can fix the optimum temperature at which MTR should be operated. We can see that the maximum efficiency always results at 840 ˚C MTR temperature. We can also conclude that the efficiency does not change much with the LTR's temperature change. Still, the change in efficiency with a change in LTR's temperature has a trend. Efficiency decreases with a decrease in LTR's temperature. Therefore, it is better to operate LTR at lowest possible temperature. But from the phase diagram (Figure-2) we know that we should operate LTR above 406˚C. Considering operational flexibility, we choose to operate LTR at 430˚C.

5.1.4.3. Mode-3

In mode-3, we explored a qualitative relationship of efficiency with HTR's temperature, keeping feed composition and all other reactors temperature constant. Figure-27 is showing the result of this sensitivity analysis.

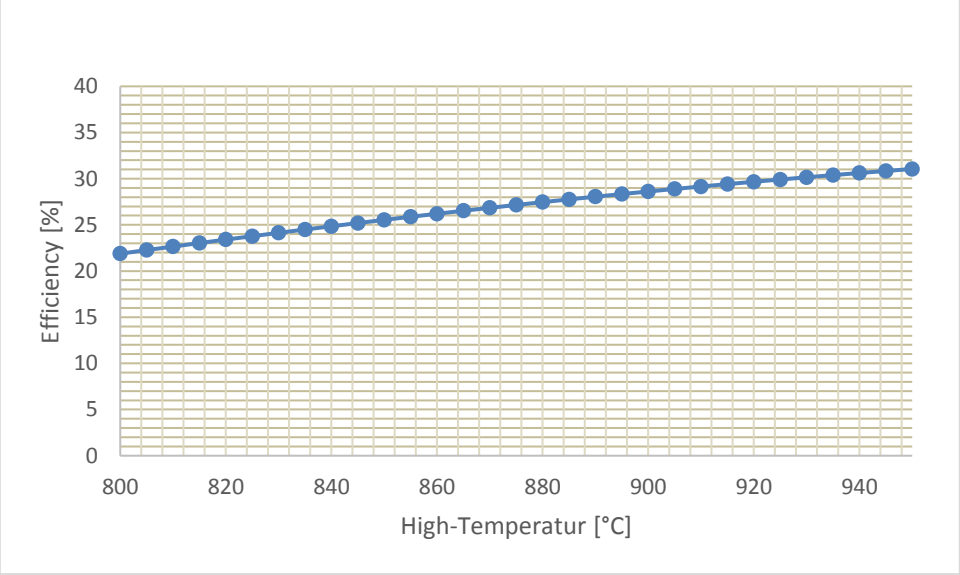

Figure 27: Sensitivity of efficiency on HTR's temperature.

We can conclude from this plot that efficiency increases with increase in temperature of the HTR. Nevertheless, it was considered material wise to remain below 900°C [37].

5.1.5. Sensitivity of efficiency on photo reactors efficiency

Besides the investigation of the sensitivity of overall efficiency on feed composition and reactor temperature, we also investigated the sensitivity of efficiency on photo reactors efficiency. We varied photo reactors efficiency from 25% to 100% at 10% interval and varied the total solar energy from 1000 MW to 4000 MW. We recorded the overall process efficiency against this two parameter variation. Figure-28 is showing the result of this analysis.

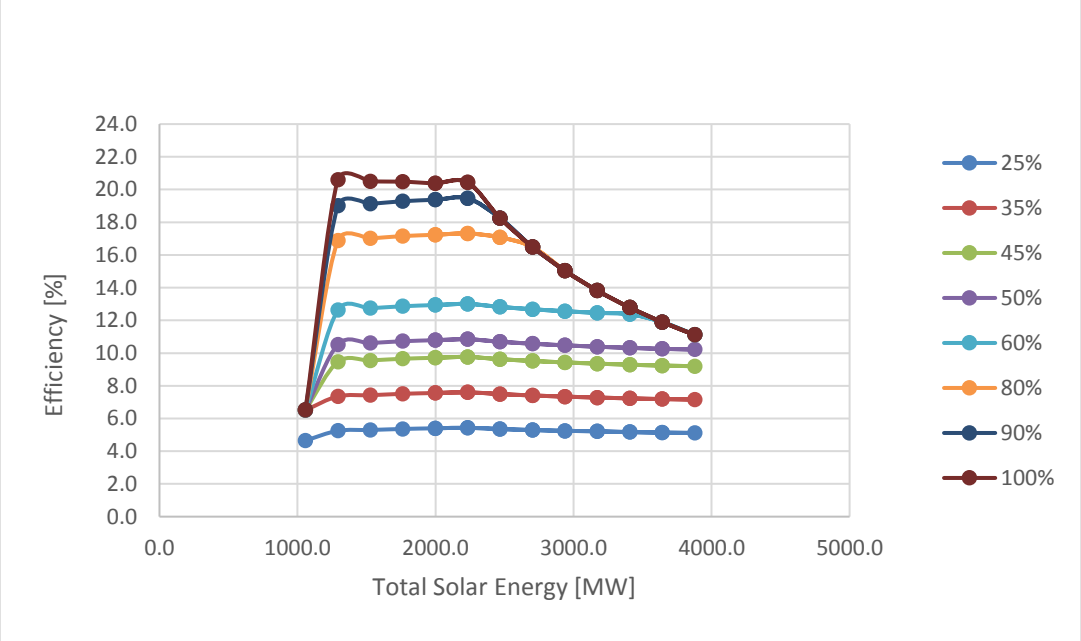

Figure 28: Sensitivity of plant efficiency on photo reactors efficiency.

We can conclude from Figure-28 that the overall plant efficiency increases as we increase photo reactor's efficiency uniformly. But almost remain same with total solar

energy. This is because the process flow sheet was designed to absorb a certain amount of solar energy and the excess energy will be discarded by defocusing the solar concentrator. We can also see that at the beginning, the efficiency of the process is dominated by thermal energy but after that only photonic energy controls the production of hydrogen, i.e. photonic energy is the limiting one.

5.2. Thermal energy storage (TES)

The second objective of this study was to integrate a TES with the process flowsheet. A conceptual model has been developed to do so. Therefore, a new flowsheet also developed that has both the previous flowsheet (Figure-24) and the TES incorporated in it. Both models are discussed in detail in the following two sub-sections.

5.2.1. Conceptual model of TES

Figure-29 is showing the conceptual model for integration of the solar thermal energy storage system with the developed process flowsheet (Figure-24). According to the model, a stored mixture of K_2SO_4-$K_2S_2O_7$ salt at 430°C or 840°C will be pumped from the thermal energy storage based on process requirements. This means cold salt will be supplied from the cold salt storage tank when solar energy is more than required to take the excess energy from the system and store it for use in later part of the day. Similarly, the hot salt will be supplied when process receive less energy than required to cover the energy shortage.

This system can only supply or store solar thermal energy not photonic, so whenever there is a shortage in the photonic energy i.e. absence of sun, this system will only help to keep the process pre-heated so that the process can start operating early in

the morning. And no hydrogen will be produced during this period. Thus this TES can shorten the start up time.

TES can supply energy to LTR and MTR, but for HTR we designed to utilize the hot SO_3 to make up the energy storage to keep HTR pre-heated.

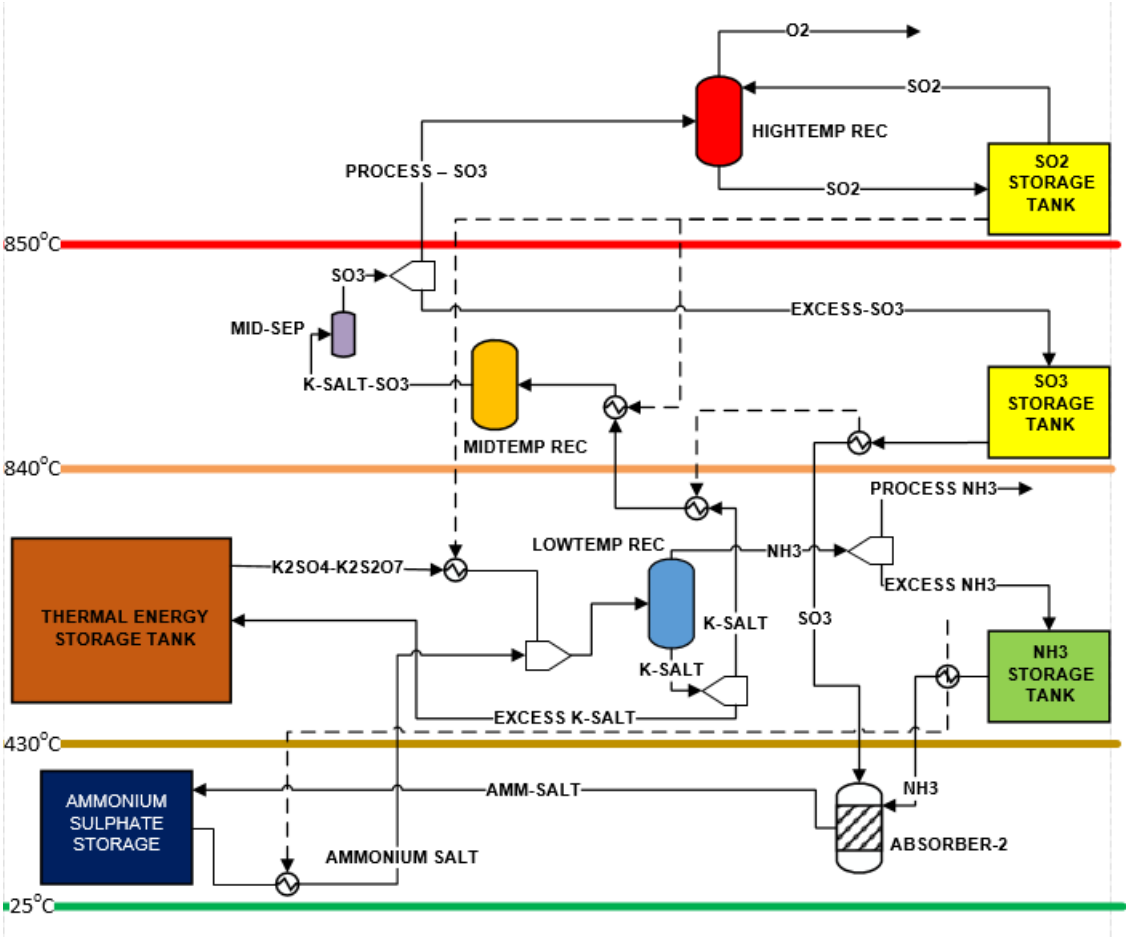

Figure 29: Conceptual model for integration of thermal storage system.

5.2.2. Process flowsheet with TES

We integrated this conceptual model with the flow sheet developed and discussed in section 5.1 by using six design specification blocks. The task of all these design specification blocks were to maintain the temperature of the concerned reactor at optimum design temperature. We modified the flowsheet in Figure-24 by adding two different salt streams to each reactor; one is to supply heat, and another is to take heat from the reactor. Figure-30 is an update of Figure-24 incorporating this concept of TES.

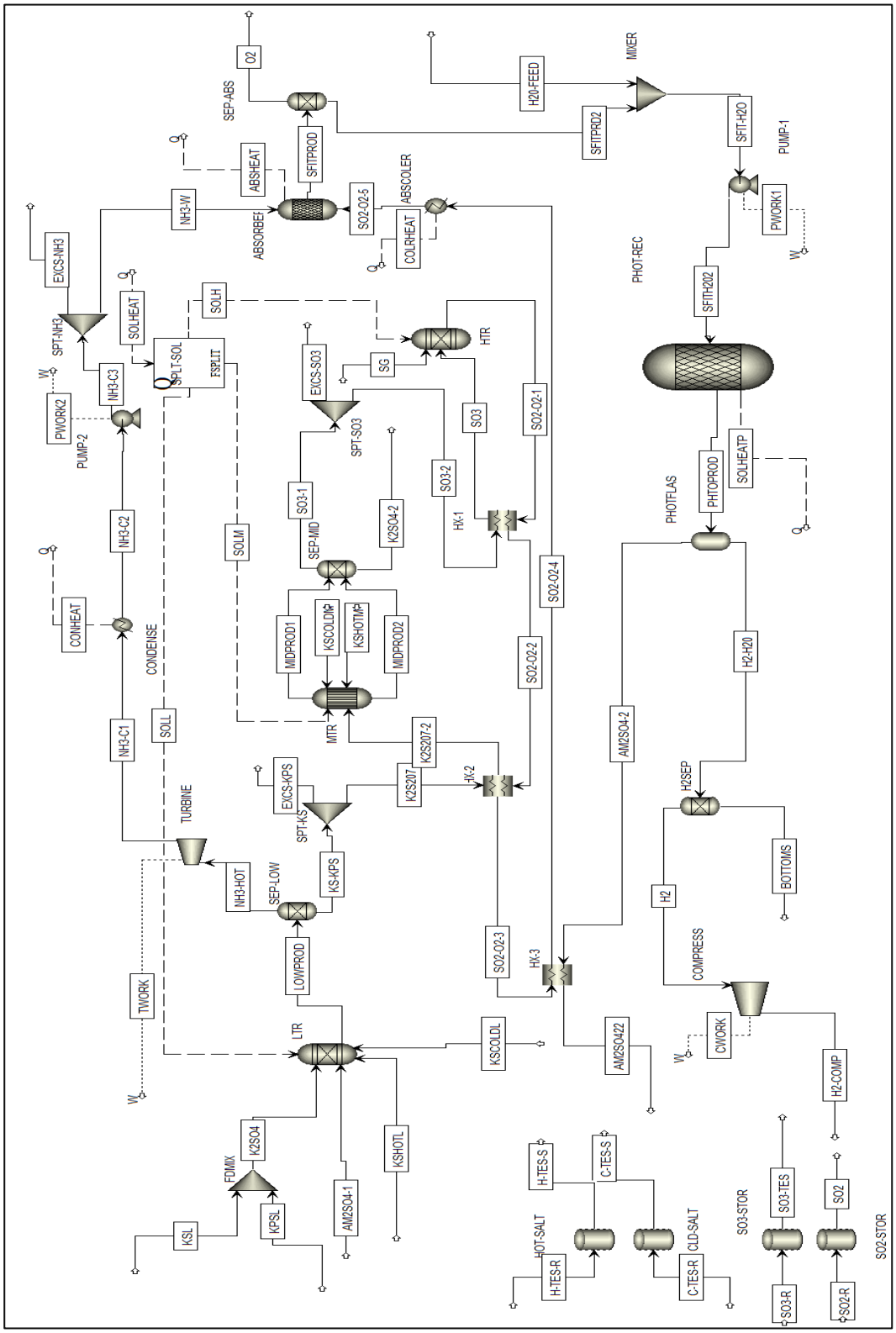

Figure 30: Process flowsheet with integrated thermal storage system

We followed all the steps for the temperature controller discussed in setting up the six design specification blocks. We ran these blocks at different hourly solar radiations. These hourly data for solar radiations were taken from literature [38]. We plotted the performance of the process against this hourly variation of solar radiation. Figure-31 is showing the result of this investigation.

According to literature, solar radiation (represented by SH in the plot) starts at 6.4 hrs. Then increase to a maximum at 12.8 hrs. After that, it continued to decrease and become zero after 16.8 hrs.

In Figur-31, the efficiency of the process demonstrated two picks. Both of these peaks resulted from the situations when system received sufficient photonic energy to produce hydrogen and a part of the thermal energy from TES. Similarly, the valley in the middle of the efficiency line resulted when the process stores a part of the solar thermal energy as sensible heat. But produce the same optimum amount of hydrogen. During the period of storing, the process produces the maximum possible amount of hydrogen and stores energy at the same time. Thus, efficiency falls from the calculated efficiency of 25.54%. The calculated average efficiency of the process for the production period with TES drops to 19.41% from the rated efficiency.

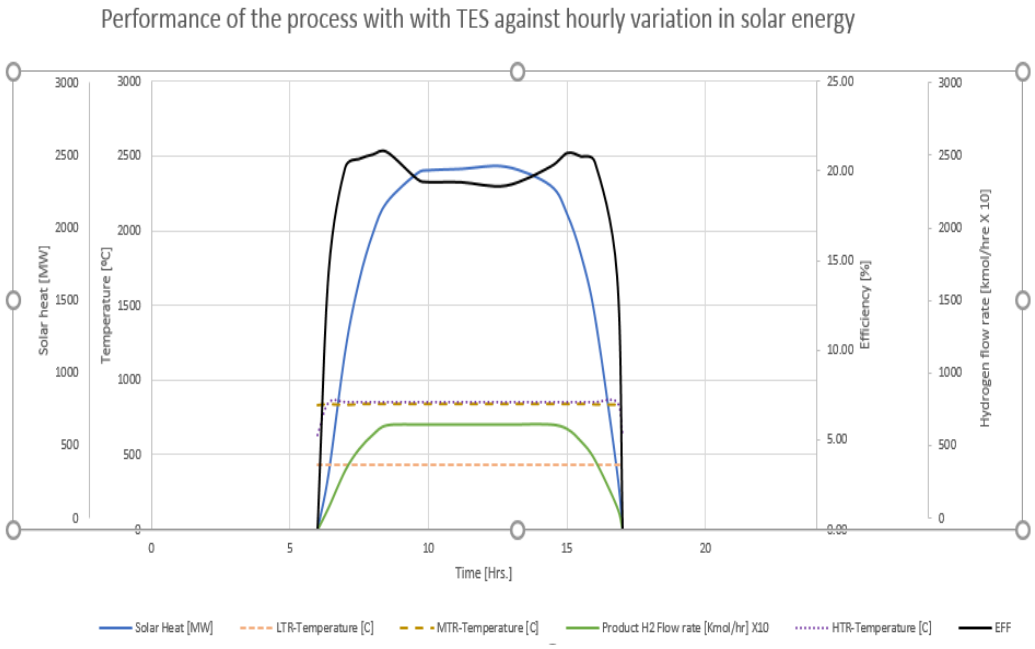

Figure 31: Process performance with the integrated solar thermal storage system.

The temperature controller (TC) of each reactor responded to the variation in heat radiation accordingly to keep the temperature of concern reactor at designed value or close to design temperature. Results of these controllers are shown in Figure-30 as reactor's temperature (LTR, MTR, and HTR). From the TC's result in Figure-30, it is evident that storage fluid can keep the temperature of the LTR and MTR at designed operating temperature. For HTR in the absence of the sun the heating fluid (SO_3) can not increase the temperature of the reactor above 629°C thus during this period, we can only keep HTR pre-heated.

We also noted from the analysis, the hourly flow rate of different cooling and heating salts. This flow rate of TES fluid is required for finding the storage tank size for

one-hour thermal support. Figure-32 is showing graphically the change in this flow rate against time. In this plot, all the flow rates are reported as kmol salt per kmol hydrogen.

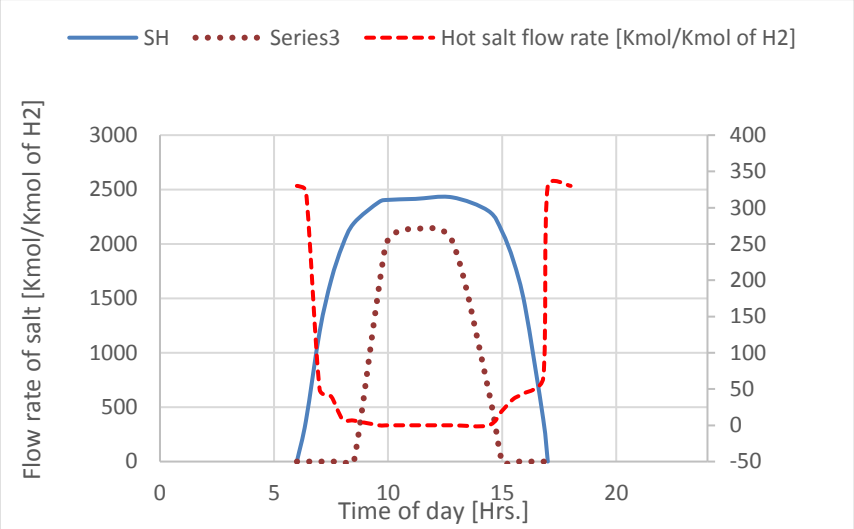

Figure 32: Hourly thermal storage flow rate for different reactors.

We found that the required maximum hot salt flow rate is 330 Kmol / Kmol H_2. And maximum cold salt flow rate is 2139 Kmol / Kmol H_2. We can use this hourly flow rate plot to find out the salt storage tank's capacity.

5.2.3. Analysis of TES performance

We conducted one more analysis to compare the performance of process with TES and process without TES. In a practical situation when the available solar energy gets more than required, the solar concentrator wastes the excess part by defocusing the mirror. We compare efficiencies of two cases considering this phenomenon. In the case of TES instead of wasting this energy, we stored it and calculated the efficiency. Figure-33 is showing the result of this analysis. In this plot, we calculated all the efficiencies are taking the efficiency of concentrator and photo reactor.

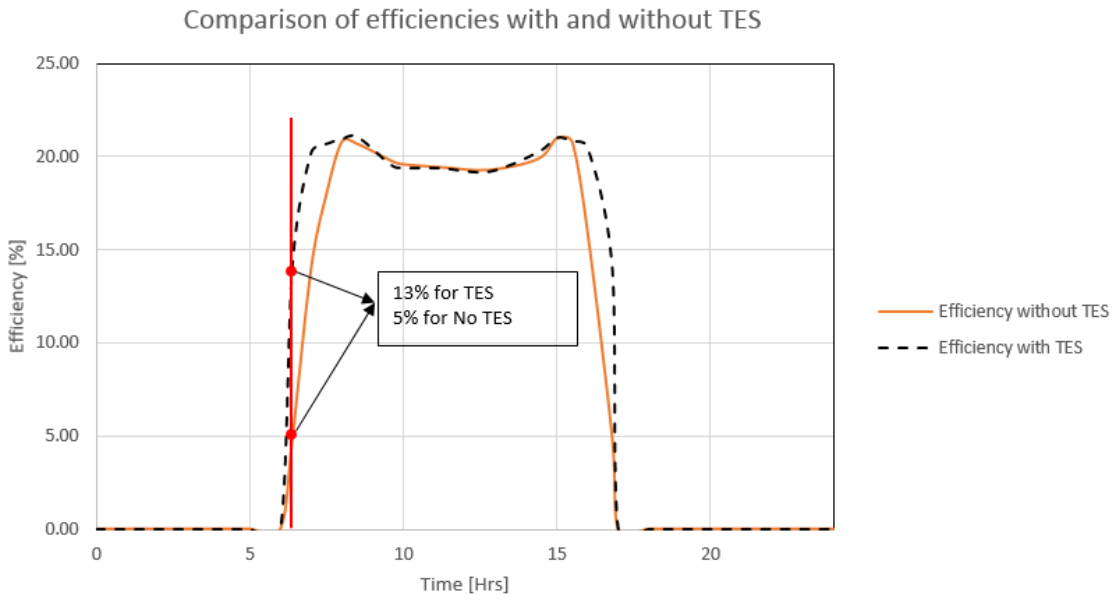

Figure 33: Compare of efficiencies of the developed process flow sheet with and without TES

From Figure-33, we can see that initially, the overall process efficiency is higher for TES integrated process. This initial high efficiency resulted because TES make up the energy shortage to produce the maximum amount of hydrogen at that time of the day.

In addition to that this plot also shows that the efficiency of the process at two different cases are identical during the period when solar energy supply is more than required (the period between the two peak). The reason for this is TES stores the same amount of energy that usually wasted in normal operation by defocusing the solar concentrator. Therefore, energy consumptions for the two scenarios are same. However, TES provides more operational stability and keeps the process pre-heated to help early production of hydrogen.

5.3. Economic analysis

Aspen Plus process simulator has built in economic analysis tools to calculate the capital cost, installation cost, operation cost and other associated costs for the preliminary economic analysis of different scenarios. Table-5 is showing a comparative cost analysis of the two scenarios i.e. one without TES and another with TES.

Costs	**Process Without TES**	**Process with TES**
Total capital investment (USD)	228201000	250454000
Total operating cost (USD/year)	4975300	4985300
Total raw material cost (USD/year)	46167600	46416300
Total product sales (USD/year)	378115000	381873000
Total utility cost (USD/year)	23023100	23431400
Equipment cost (USD)	884690000	1052186000
Total installation cost (USD)	120314000	150237000
Calculated IRR (%)	24.44	20.75

Table 5: Comparative cost analysis of the process with and without TES.

From this comparison, we can conclude that the process requires $22.2 M more capital investment, $167.5 M more expense for equipment and $29.9 M more investment for equipment installation, to integrate a TES. While this upgrade will result in an increase in annual revenue of $3.7 M. However, to compare the two option the internal rate of return (IRR) must for each cash flow must be greater than the Minimum Acceptable Rate of Return (MARR). In most common cases, the MARR is 20%. So we can see from Table-5 that for both cash flow option IRR>MARR. Therefore, both option is economically feasible.

However, two compare these two cash flow we need to subtract first cash flow from the second one and calculate IRR for the new cash flow. If IRR for this cash flow is greater than MARR, then the extra investment to upgrade the process to a TES integrated one is economically advantageous. We compared these two cash flows and calculated the IRR. We find out that IRR<MARR for the compared cash flow. Therefore, we can conclude that extra investment is not economically feasible.

6. CONCLUSIONS AND RECOMMENDATIONS

The main objective of this process was to determine the overall viability of the sulfur ammonia solar-photo-thermochemical hydrogen production process and to integrate a solar thermal energy storage system with developed process flow sheet. This includes first to converge the material and energy balance of the flowsheet and run several sensitivity analysis. Then find the feasibility of integration of the thermal energy storage system.

Integration of TES was a big challenge, as we wanted to use the process fluid as the storage fluid by adding it directly to the system along with the feed streams. Then separate this excess salt from the product streams. Figure-29 is a conceptual model of this idea. In this model, we used salt streams of two different temperature to work as a heating and cooling fluid.

The material and energy balance sheet (Table 1 and 2) shows that the difference between the input and output material and energy flow is 0.00% for both cases. This indicates the convergence of the process flow sheet.

The final developed flow sheet for solar photo thermochemical process (Figure-24) and same process with TES (Figure-30) shows all the equipments and other specification blocks we needed to complete the process and run a different analysis of the process. In this study, we designed all the reactors to follow the K_2SO_4-$K_2S_2O_7$ salt phase diagram (Figure-2) to ensure complete liquid operation. The optimum temperature of Low-temperature (430˚C) and Mid-temperature (840˚C) reactor were determined

from this phase diagram and sensitivity analysis of efficiency. In addition, we designed the process to operate at 9 bar pressure, same as the phase diagram plot.

We used a calculator block to find out the efficiency of both process scenarios. We find out when we run the process without thermal energy storage system the steady state efficiency is 25.57%. In the case of process with TES, we calculated the average efficiency. Since the solar radiation will vary over time; process efficiency will also vary thus there is no fixed efficiency of the process. During the productive period, the average calculated efficiency is 19.41% with TES.

Both of these efficiencies were calculated without taking into account the solar to solar thermal conversion and solar photonic to hydrogen conversion efficiencies. We corrected the calculated efficiency with this conversion efficiencies and obtained 12.55% final steady state efficiency.

One similar previous study of Sulfur ammonia cycle (Littlefield et.el, 2012), with an electrolyzer in the process instead of a photo reactor. This study reported 23% overall process efficiency. In this study in calculating the overall efficiency, released energy was from absorber was consider as useful energy. The energy released from the absorber is not convertible to useful energy as absorber operates at 25 ˚C. Also, Littlefield did not consider solar to solar thermal conversion efficiency. In our study, if we followed the same procedure as literature, an overall process efficiency of 60.3% would result.

The designed thermal energy storage system requires hourly 330 kmol hot salt/kmol product hydrogen and 2139 kmol cold salt/kmol product hydrogen. We also

performed an economic comparison of the two options i.e. one without TES and with TES.

The process requires $219.7 M more investment to upgrade the process a TES integrated process and this extra investment will increase $3.7 M annual revenue. However, comparative study of the two option showed that this extra investment does not offer any extra economic benefit.

Although these preliminary results are positive, more studies are required to incorporate more laboratory data to make the simulation more realistic. In all the reactions, the reaction kinetics must be obtained by performing laboratory experiments so that the actual effects of net duty change across each reactor can be investigated.

In the case of designing the thermal energy storage system, we could not investigate how the process will perform after an hour of operation i.e. how the temperature profile of different storage salts will change. Thus, we could not simulate temperature change in the storage tank after one hour of operation. A dynamic simulation of the process is required to do so.

The developed process flow sheet is only a preliminary design of the HySA process, but through more study and integration of more practical data, this flow sheet can become a useful tool to design a full-scale hydrogen production plant.

REFERENCES

[1] Rosen MA. Advances in hydrogen production by thermochemical water decomposition: A review. Energy 2010;35:1068–76. doi:10.1016/j.energy.2009.06.018.

[2] Abanades S, Charvin P, Flamant G, Neveu P. Screening of water-splitting thermochemical cycles potentially attractive for hydrogen production by concentrated solar energy. Energy 2006;31:2469–86. doi:10.1016/j.energy.2005.11.002.

[3] Xiao L, Wu SY, Li YR. Advances in solar hydrogen production via two-step water-splitting thermochemical cycles based on metal redox reactions. Renew Energy 2012;41:1–12. doi:10.1016/j.renene.2011.11.023.

[4] T-Raissi A, Muradov N, Huang C, Adebiyi O. Hydrogen From Solar Via Light-Assisted High-Temperature Water Splitting Cycles. J Sol Energy Eng 2007;129:184. doi:10.1115/1.2710493.

[5] Chen Y., Chong K., Lim C., Lim B., Tan K., Aliman O, et al. Report of the first prototype of non-imaging focusing heliostat and its application in high temperature solar furnace. Sol Energy 2002;72:531–44. doi:10.1016/S0038-092X(02)00028-2.

[6] Steinfeld A. Solar hydrogen production via a two-step water-splitting thermochemical cycle based on Zn/ZnO redox reactions. Int J Hydrogen Energy 2002;27:611–9. doi:10.1016/S0360-3199(01)00177-X.

[7] Steinfeld A, Sanders S, Palumbo R. Design Aspects of Solar Thermochemical

Engineering—A Case Study: Two-Step Water-Splitting Cycle Using The Fe3O4/FeO Redox System. Sol Energy 1999;65:43–53. doi:10.1016/S0038-092X(98)00092-9.

[8] Zamfirescu C, Dincer I, Naterer GF. Thermophysical properties of copper compounds in copper-chlorine thermochemical water splitting cycles. Int J Hydrogen Energy 2010;35:4839–52. doi:10.1016/j.ijhydene.2009.08.101.

[9] Naterer GF, Gabriel K, Wang ZL, Daggupati VN, Gravelsins R. Thermochemical hydrogen production with a copper-chlorine cycle. I: oxygen release from copper oxychloride decomposition. Int J Hydrogen Energy 2008;33:5439–50. doi:10.1016/j.ijhydene.2008.05.035.

[10] Kasahara S, Kubo S, Hino R, Onuki K, Nomura M, Nakao S ichi. Flowsheet study of the thermochemical water-splitting iodine-sulfur process for effective hydrogen production. Int J Hydrogen Energy 2007;32:489–96. doi:10.1016/j.ijhydene.2006.05.005.

[11] Wang ZL, Naterer GF, Gabriel KS, Gravelsins R, Daggupati VN. Comparison of sulfur-iodine and copper-chlorine thermochemical hydrogen production cycles. Int J Hydrogen Energy 2010;35:4820–30. doi:10.1016/j.ijhydene.2009.09.006.

[12] Taylor R, Davenport R, Talbot J, Herz R, Luc W, Genders D, et al. Status of the solar sulfur ammonia thermochemical hydrogen production system for splitting water. Energy Procedia 2013;49:2047–58. doi:10.1016/j.egypro.2014.03.217.

[13] Littlefield J, Wang M, Brown LC, Herz RK, Talbot JB. Process modeling and thermochemical experimental analysis of a solar sulfur ammonia hydrogen

production cycle. Energy Procedia 2012;29:616–23. doi:10.1016/j.egypro.2012.09.071.

[14] Kalyva AE, Vagia EC, Konstandopoulos a G, Srinivasa AR, T-Raissi A, Muradov N, et al. Investigation of the solar hybrid photo-thermochemical sulfur-ammonia water splitting cycle for hydrogen production. Chem Eng Trans 2015;45:361–6. doi:10.3303/CET1545061.

[15] Kalyva AE, Vagia EC, Konstandopoulos AG, Srinivasa AR, T-Raissi A, Muradov N, et al. Particle model investigation for the thermochemical steps of the sulfur–ammonia water splitting cycle. Int J Hydrogen Energy 2017;42:3621–9. doi:10.1016/j.ijhydene.2016.09.003.

[16] Zhang Y, Chen J, Xu C, Zhou K, Wang Z, Zhou J, et al. A novel photo-thermochemical cycle of water-splitting for hydrogen production based on TiO2-x/TiO2. Int J Hydrogen Energy 2016;41:2215–21. doi:10.1016/j.ijhydene.2015.12.067.

[17] Lefebvre D, Tezel FH. A review of energy storage technologies with a focus on adsorption thermal energy storage processes for heating applications. Renew Sustain Energy Rev 2017;67:116–25. doi:10.1016/j.rser.2016.08.019.

[18] Li J, Cheng X, Shashurin A, Keidar M. Review of Electrochemical Capacitors Based on Carbon Nanotubes and Graphene. Graphene 2012;1:1–13. doi:10.4236/graphene.2012.11001.

[19] De Gracia A, Cabeza LF. Phase change materials and thermal energy storage for buildings. Energy Build 2015;103:414–9. doi:10.1016/j.enbuild.2015.06.007.

[20] Hasnain S.M. Review on sustainable thermal energy storage technologies, Part I: heat storage materials and techniques. Energy Convers Manag 1998;39:1127–38. doi:10.1016/S0196-8904(98)00025-9.

[21] Abedin AH. Thermochemical energy storage systems: Modelling, analysis and design. vol. M. Sc. Elsevier Inc.; 2010. doi:10.1016/B978-0-12-803440-8/00017-8.

[22] Shigeishi RA, Langford CH, Hollebone BR. Solar energy storage using chemical potential changes associated with drying of zeolites. Sol Energy 1979;23:489–95. doi:10.1016/0038-092X(79)90072-0.

[23] Huang X, Alva G, Jia Y, Fang G. Morphological characterization and applications of phase change materials in thermal energy storage: A review. Renew Sustain Energy Rev 2017;72:128–45. doi:10.1016/j.rser.2017.01.048.

[24] Sharma A, Tyagi V V., Chen CR, Buddhi D. Review on thermal energy storage with phase change materials and applications. Renew Sustain Energy Rev 2009;13:318–45. doi:10.1016/j.rser.2007.10.005.

[25] Pinel P, Cruickshank CA, Beausoleil-Morrison I, Wills A. A review of available methods for seasonal storage of solar thermal energy in residential applications. Renew Sustain Energy Rev 2011;15:3341–59. doi:10.1016/j.rser.2011.04.013.

[26] Zalba B, Mar??n JM, Cabeza LF, Mehling H. Review on thermal energy storage with phase change: Materials, heat transfer analysis and applications. vol. 23. 2003. doi:10.1016/S1359-4311(02)00192-8.

[27] Hariri AS, Ward IC. A review of thermal storage systems used in building

applications. Build Environ 1988;23:1–10. doi:10.1016/0360-1323(88)90011-X.

[28] Steinmann WD, Eck M. Buffer storage for direct steam generation. Sol Energy 2006;80:1277–82. doi:10.1016/j.solener.2005.05.013.

[29] Hänchen M, Brückner S, Steinfeld A. High-temperature thermal storage using a packed bed of rocks - Heat transfer analysis and experimental validation. Appl Therm Eng 2011;31:1798–806. doi:10.1016/j.applthermaleng.2010.10.034.

[30] Medrano M, Gil A, Martorell I, Potau X, Cabeza LF. State of the art on high-temperature thermal energy storage for power generation. Part 2-Case studies. Renew Sustain Energy Rev 2010;14:56–72. doi:10.1016/j.rser.2009.07.036.

[31] DeLaquil P, Kelly B, Lessley R. Solar One Conversion Project. Sol Energy Mater 1991;24:151–61.

[32] Lindberg D, Backman R, Chartrand P. Thermodynamic evaluation and optimization of the (Na2SO4 + K2SO4 + Na2S2O7 + K2S2O7) system. J Chem Thermodyn 2006;38:1568–83. doi:10.1016/j.jct.2006.04.002.

[33] Kalyva AE, Vagia EC, Konstandopoulos AG, Srinivasa AR, T-raissi A. Hybrid photo-thermal sulfur-ammonia water splitting cycle : Thermodynamic analysis of the lower temperature thermochemical steps n.d.

[34] Green DW, Perry RH. Perry's Chemical Engineer Handbook. 8th ed. McGraw-Hill: New York, Chicago, San Francisco, Lisbon, London, Madrid, Mexico City, Milan, New Delhi, San Juan, Seoul, Singapore, Sydney, Toronto; n.d.

[35] T-Raissi A, Huang C, Muradov N. Hydrogen production by solar thermo-chemical water splitting 2004:502704.

[36] Eschenbache TG, Lewis NA, Hartman JC, Bussey LE. The Economic Analysis of Industrial Projects. Third Edit. OXFORD; n.d.

[37] Pardo P, Deydier A, Anxionnaz-Minvielle Z, Rougé S, Cabassud M, Cognet P. A review on high temperature thermochemical heat energy storage. Renew Sustain Energy Rev 2014;32:591–610. doi:10.1016/j.rser.2013.12.014.

[38] Bachour D, Perez-Astudillo D. Boundary layer height measurements over Doha using Lidar. Energy Procedia 2014;57:1086–91. doi:10.1016/j.egypro.2014.10.094.

APPENDIX

A. Complete Stream table for steady-state simulation

A.1. Molar flow rate stream table

	Units	AM2SO4-1	AM2SO4-2	AM2SO422	BOTTOMS	EXCS-KPS	EXCS-NH3	EXCS-SO2
From			PHOTFLAS	HX-3	H2SEP	SPT-KS	SPT-NH3	SPT-SO2
To		LTR	HX-3					
Substream: MIXED								
Phase: All								
Component Mole Flow								
K2SO4	KMOL/HR	0.00	0.00	0.00	0.00	6821.27	0.00	0.00
K2S2O7	KMOL/HR	0.00	0.00	0.00	0.00	202258.00	0.00	0.00
NH4)2SO4	KMOL/HR	11800.00	11799.68	11799.68	0.00	0.00	0.00	0.00
NH4)2S03	KMOL/HR	368.37	368.69	368.69	0.00	0.00	0.00	0.00
NH3	KMOL/HR	0.00	0.00	0.00	0.00	0.00	0.00	0.00
H2O	KMOL/HR	1250.00	1249.89	1249.89	21.20	0.00	0.00	0.00
SO3	KMOL/HR	0.00	0.00	0.00	0.00	0.00	0.00	0.02
S02	KMOL/HR	0.00	0.43	0.43	0.89	0.00	0.00	0.03
H2SO4	KMOL/HR	0.00	0.00	0.00	0.00	0.00	0.00	0.00
O2	KMOL/HR	0.00	0.00	0.00	0.00	0.00	0.00	0.02
H2	KMOL/HR	0.00	0.94	0.94	0.00	0.00	0.00	0.00
KS2	KMOL/HR	0.00	0.00	0.00	0.00	0.00	0.00	0.00
KS1	KMOL/HR	0.00	0.00	0.00	0.00	0.00	0.00	0.00
KPS	KMOL/HR	0.00	0.00	0.00	0.00	0.00	0.00	0.00
AHSS	KMOL/HR	0.00	0.00	0.00	0.00	0.00	0.00	0.00
AHSL	KMOL/HR	0.00	0.00	0.00	0.00	0.00	0.00	0.00
Temperature	C	110.00	25.00	80.00	25.00	430.02	20.10	850.00
Pressure	BAR	9.00	1.00	9.00	9.00	9.00	10.00	9.00
Mole Flow	KMOL/HR	13418.37	13419.64	13419.64	22.09	209079.00	0.00	0.07

A.1. Molar flow rate stream table (continued)

	Units	EXCS-SO3	H2	H20-FEED	H2-COMP	H2-H20	K2S207	K2S207-2
From		SPT-SO3	H2SEP		COMPRESS	PHOTFLAS	SPT-KS	HX-2
To			COMPRESS	MIXER		H2SEP	HX-2	MTR
Substream: MIXED								
Phase: All								
Component Mole Flow								
K2SO4	KMOL/HR	0.00	0.00	0.00	0.00	0.00	2008.08	2008.08
K2S2O7	KMOL/HR	0.00	0.00	0.00	0.00	0.00	59541.92	59541.92
NH4)2SO4	KMOL/HR	0.00	0.00	0.00	0.00	0.00	0.00	0.00
NH4)2S03	KMOL/HR	0.00	0.00	0.00	0.00	0.00	0.00	0.00
NH3	KMOL/HR	0.00	0.00	0.00	0.00	0.00	0.00	0.00
H2O	KMOL/HR	0.00	0.00	7026.20	0.00	21.20	0.00	0.00
SO3	KMOL/HR	0.13	0.00	0.00	0.00	0.00	0.00	0.00
S02	KMOL/HR	0.00	0.00	0.00	0.00	0.89	0.00	0.00
H2SO4	KMOL/HR	0.00	0.00	0.00	0.00	0.00	0.00	0.00
O2	KMOL/HR	0.00	0.00	0.00	0.00	0.00	0.00	0.00
H2	KMOL/HR	0.00	7004.17	0.00	7004.17	7004.17	0.00	0.00
KS2	KMOL/HR	0.00	0.00	0.00	0.00	0.00	0.00	0.00
KS1	KMOL/HR	0.00	0.00	0.00	0.00	0.00	0.00	0.00
KPS	KMOL/HR	0.00	0.00	0.00	0.00	0.00	0.00	0.00
AHSS	KMOL/HR	0.00	0.00	0.00	0.00	0.00	0.00	0.00
AHSL	KMOL/HR	0.00	0.00	0.00	0.00	0.00	0.00	0.00
Temperature	C	800.00	25.00	25.00	160.49	25.00	430.02	820.00
Pressure	BAR	9.00	9.00	9.00	20.68	1.00	9.00	9.00
Mole Flow	KMOL/HR	0.13	7004.17	7026.20	7004.17	7026.26	61550.00	61550.00

A.1. Molar flow rate stream table (continued)

	Units	K2SO4	K2SO4-2	KPSL	KS-KPS	KSL	LOWPROD	MIDPROD1
From		FDMIX	SEP-MID		SEP-LOW		LTR	MTR
To		LTR		FDMIX	SPT-KS	FDMIX	SEP-LOW	SEP-MID
Substream: MIXED								
Phase: All								
Component Mole Flow								
K2SO4	KMOL/HR	20629.35	13809.59	0.00	8829.35	20629.35	8829.35	0.00
K2S2O7	KMOL/HR	250000.00	47740.41	250000.00	261800.00	0.00	261800.00	0.00
NH4)2SO4	KMOL/HR	0.00	0.00	0.00	0.00	0.00	0.00	0.00
NH4)2S03	KMOL/HR	0.00	0.00	0.00	0.00	0.00	0.00	0.00
NH3	KMOL/HR	0.00	0.00	0.00	0.00	0.00	24336.74	0.00
H2O	KMOL/HR	0.00	0.00	0.00	0.00	0.00	13418.37	0.00
SO3	KMOL/HR	0.00	0.00	0.00	0.00	0.00	0.00	11697.04
S02	KMOL/HR	0.00	0.00	0.00	0.00	0.00	368.37	0.00
H2SO4	KMOL/HR	0.00	0.00	0.00	0.00	0.00	0.00	0.00
O2	KMOL/HR	0.00	0.00	0.00	0.00	0.00	0.00	0.00
H2	KMOL/HR	0.00	0.00	0.00	0.00	0.00	0.00	0.00
KS2	KMOL/HR	0.00	0.00	0.00	0.00	0.00	0.00	0.00
KS1	KMOL/HR	0.00	0.00	0.00	0.00	0.00	0.00	0.00
KPS	KMOL/HR	0.00	0.00	0.00	0.00	0.00	0.00	0.00
AHSS	KMOL/HR	0.00	0.00	0.00	0.00	0.00	0.00	0.00
AHSL	KMOL/HR	0.00	0.00	0.00	0.00	0.00	0.00	0.00
Temperature	C	430.00	800.00	430.00	430.02	430.00	430.02	840.00
Pressure	BAR	9.00	9.00	9.00	9.00	9.00	9.00	9.00
Mole Flow	KMOL/HR	270629.00	61550.00	250000.00	270629.00	20629.35	308753.00	11697.04

A.1. Molar flow rate stream table (continued)

	Units	MIDPROD2	NH3-C1	NH3-C2	NH3-C3	NH3-HOT	NH3-W	O2
From		MTR	TURBINE	CONDENSE	PUMP-2	SEP-LOW	SPT-NH3	SEP-ABS
To		SEP-MID	CONDENSE	PUMP-2	SPT-NH3	TURBINE	ABSORBER	
Substream: MIXED								
Phase: All								
Component Mole Flow								
K2SO4	KMOL/HR	13809.59	0.00	0.00	0.00	0.00	0.00	0.00
K2S2O7	KMOL/HR	47740.41	0.00	0.00	0.00	0.00	0.00	0.00
NH4)2SO4	KMOL/HR	0.00	0.00	0.00	0.00	0.00	0.00	0.00
NH4)2S03	KMOL/HR	0.00	0.00	0.00	0.00	0.00	0.00	0.00
NH3	KMOL/HR	0.00	24336.74	24336.74	24336.74	24336.74	24336.74	0.00
H2O	KMOL/HR	0.00	13418.37	13418.37	13418.37	13418.37	13418.37	0.00
SO3	KMOL/HR	104.47	0.00	0.00	0.00	0.00	0.00	0.00
S02	KMOL/HR	0.00	368.37	368.37	368.37	368.37	368.37	0.00
H2SO4	KMOL/HR	0.00	0.00	0.00	0.00	0.00	0.00	0.00
O2	KMOL/HR	0.00	0.00	0.00	0.00	0.00	0.00	3503.38
H2	KMOL/HR	0.00	0.00	0.00	0.00	0.00	0.00	0.00
KS2	KMOL/HR	0.00	0.00	0.00	0.00	0.00	0.00	0.00
KS1	KMOL/HR	0.00	0.00	0.00	0.00	0.00	0.00	0.00
KPS	KMOL/HR	0.00	0.00	0.00	0.00	0.00	0.00	0.00
AHSS	KMOL/HR	0.00	0.00	0.00	0.00	0.00	0.00	0.00
AHSL	KMOL/HR	0.00	0.00	0.00	0.00	0.00	0.00	0.00
Temperature	C	840.00	196.35	20.00	20.10	430.02	20.10	25.00
Pressure	BAR	9.00	0.40	5.00	10.00	9.00	10.00	9.00
Mole Flow	KMOL/HR	61654.46	38123.48	38123.48	38123.48	38123.48	38123.48	3503.38

A.1. Molar flow rate stream table (continued)

	Units	PHTOPROD	SFITH202	SFIT-H2O	SFITPRD2	SFITPROD	SO2-02-6	SO2-O2-1
From		PHOT-REC	PUMP-1	MIXER	SEP-ABS	ABSORBER	HTR	SPT-SO2
To		PHOTFLAS	PHOT-REC	PUMP-1	MIXER	SEP-ABS	SPT-SO2	HX-1
Substream: MIXED								
Phase: All								
Component Mole Flow								
K2SO4	KMOL/HR	0.00	0.00	0.00	0.00	0.00	0.00	0.00
K2S2O7	KMOL/HR	0.00	0.00	0.00	0.00	0.00	0.00	0.00
NH4)2SO4	KMOL/HR	11799.68	4794.57	4794.57	4794.57	4794.57	0.00	0.00
NH4)2S03	KMOL/HR	368.69	7373.80	7373.80	7373.80	7373.80	0.00	0.00
NH3	KMOL/HR	0.00	0.00	0.00	0.00	0.00	0.00	0.00
H2O	KMOL/HR	1271.09	8276.20	8276.20	1250.00	1250.00	0.00	0.00
SO3	KMOL/HR	0.00	0.00	0.00	0.00	0.00	4794.59	4794.57
S02	KMOL/HR	1.33	1.33	1.33	1.33	1.33	7006.79	7006.75
H2SO4	KMOL/HR	0.00	0.00	0.00	0.00	0.00	0.00	0.00
O2	KMOL/HR	0.00	0.00	0.00	0.00	3503.38	3503.39	3503.38
H2	KMOL/HR	7005.11	0.00	0.00	0.00	0.00	0.00	0.00
KS2	KMOL/HR	0.00	0.00	0.00	0.00	0.00	0.00	0.00
KS1	KMOL/HR	0.00	0.00	0.00	0.00	0.00	0.00	0.00
KPS	KMOL/HR	0.00	0.00	0.00	0.00	0.00	0.00	0.00
AHSS	KMOL/HR	0.00	0.00	0.00	0.00	0.00	0.00	0.00
AHSL	KMOL/HR	0.00	0.00	0.00	0.00	0.00	0.00	0.00
Temperature	C	79.73	25.27	25.00	25.00	25.00	850.00	850.00
Pressure	BAR	9.00	9.00	7.00	9.00	9.00	9.00	9.00
Mole Flow	KMOL/HR	20445.89	20445.89	20445.89	13419.69	16923.07	15304.77	15304.70

A.1. Molar flow rate stream table (continued)

	Units	SO2-O2-2	SO2-O2-3	SO2-O2-4	SO2-O2-5	SO3	SO3-1	SO3-2
From		HX-1	HX-2	HX-3	ABSCOLER	HX-1	SEP-MID	SPT-SO3
To		HX-2	HX-3	ABSCOLER	ABSORBER	HTR	SPT-SO3	HX-1
Substream: MIXED								
Phase: All								
Component Mole Flow								
K2SO4	KMOL/HR	0.00	0.00	0.00	0.00	0.00	0.00	0.00
K2S2O7	KMOL/HR	0.00	0.00	0.00	0.00	0.00	0.00	0.00
NH4)2SO4	KMOL/HR	0.00	0.00	0.00	0.00	0.00	0.00	0.00
NH4)2S03	KMOL/HR	0.00	0.00	0.00	0.00	0.00	0.00	0.00
NH3	KMOL/HR	0.00	0.00	0.00	0.00	0.00	0.00	0.00
H2O	KMOL/HR	0.00	0.00	0.00	0.00	0.00	0.00	0.00
SO3	KMOL/HR	4794.57	4794.57	4794.57	4794.57	11801.38	11801.51	11801.38
S02	KMOL/HR	7006.75	7006.75	7006.75	7006.75	0.00	0.00	0.00
H2SO4	KMOL/HR	0.00	0.00	0.00	0.00	0.00	0.00	0.00
O2	KMOL/HR	3503.38	3503.38	3503.38	3503.38	0.00	0.00	0.00
H2	KMOL/HR	0.00	0.00	0.00	0.00	0.00	0.00	0.00
KS2	KMOL/HR	0.00	0.00	0.00	0.00	0.00	0.00	0.00
KS1	KMOL/HR	0.00	0.00	0.00	0.00	0.00	0.00	0.00
KPS	KMOL/HR	0.00	0.00	0.00	0.00	0.00	0.00	0.00
AHSS	KMOL/HR	0.00	0.00	0.00	0.00	0.00	0.00	0.00
AHSL	KMOL/HR	0.00	0.00	0.00	0.00	0.00	0.00	0.00
Temperature	C	830.00	823.08	665.13	25.00	819.41	800.00	800.00
Pressure	BAR	9.00	9.00	9.00	9.00	9.00	9.00	9.00
Mole Flow	KMOL/HR	15304.70	15304.70	15304.70	15304.70	11801.38	11801.51	11801.38

A.2. Mass flow rate stream table

	Units	AM2SO4-1	AM2SO4-2	AM2SO422	BOTTOMS	EXCS-KPS	EXCS-NH3	EXCS-SO2
From			PHOTFLAS	HX-3	H2SEP	SPT-KS	SPT-NH3	SPT-SO2
To		LTR	HX-3					
Component Mass Flow								
K2SO4	KG/HR	0.0	0.0	0.0	0.0	1188680.0	0.0	0.0
K2S2O7	KG/HR	0.0	0.0	0.0	0.0	51439200.0	0.0	0.0
NH4)2SO4	KG/HR	1559260.0	1559220.0	1559220.0	0.0	0.0	0.0	0.0
NH4)2S03	KG/HR	42783.1	42820.1	42820.1	0.0	0.0	0.0	0.0
NH3	KG/HR	0.0	0.0	0.0	0.0	0.0	0.0	0.0
H2O	KG/HR	22519.1	22517.2	22517.2	381.9	0.0	0.0	0.0
SO3	KG/HR	0.0	0.0	0.0	0.0	0.0	0.0	1.8
S02	KG/HR	0.0	27.9	27.9	57.0	0.0	0.0	2.1
H2SO4	KG/HR	0.0	0.0	0.0	0.0	0.0	0.0	0.0
O2	KG/HR	0.0	0.0	0.0	0.0	0.0	0.0	0.5
H2	KG/HR	0.0	1.9	1.9	0.0	0.0	0.0	0.0
KS2	KG/HR	0.0	0.0	0.0	0.0	0.0	0.0	0.0
KS1	KG/HR	0.0	0.0	0.0	0.0	0.0	0.0	0.0
KPS	KG/HR	0.0	0.0	0.0	0.0	0.0	0.0	0.0
AHSS	KG/HR	0.0	0.0	0.0	0.0	0.0	0.0	0.0
AHSL	KG/HR	0.0	0.0	0.0	0.0	0.0	0.0	0.0
Mass Flow	KG/HR	1624560.0	1624580.0	1624580.0	438.9	52627800.0	0.1	4.5
Volume Flow	CUM/HR	3554.2	3489.8	3531.1	0.4	81589.1	0.0	0.8
Temperature	C	110.0	25.0	80.0	25.0	430.0	20.1	850.0
Pressure	BAR	9.0	1.0	9.0	9.0	9.0	10.0	9.0
Vapor Fraction		0.0	0.0	0.0	0.0	0.0	0.0	1.0
Liquid Fraction		1.0	1.0	1.0	1.0	1.0	1.0	0.0
Solid Fraction		0.0	0.0	0.0	0.0	0.0	0.0	0.0
Average Molecular Weight		121.1	121.1	121.1	19.9	251.7	17.8	121.1

A.2. Mass flow rate stream table (continued)

	Units	EXCS-SO3	H2	H20-FEED	H2-COMP	H2-H20	K2S207	K2S207-2
From		SPT-SO3	H2SEP		COMPRESS	PHOTFLAS	SPT-KS	HX-2
To			COMPRESS	MIXER		H2SEP	HX-2	MTR
Substream: MIXED								
Phase: All								
Component Mass Flow								
K2SO4	KG/HR	0.0	0.0	0.0	0.0	0.0	349929.0	349929.0
K2S2O7	KG/HR	0.0	0.0	0.0	0.0	0.0	15143000.0	15143000.0
NH4)2SO4	KG/HR	0.0	0.0	0.0	0.0	0.0	0.0	0.0
NH4)2S03	KG/HR	0.0	0.0	0.0	0.0	0.0	0.0	0.0
NH3	KG/HR	0.0	0.0	0.0	0.0	0.0	0.0	0.0
H2O	KG/HR	0.0	0.0	126579.0	0.0	381.9	0.0	0.0
SO3	KG/HR	10.3	0.0	0.0	0.0	0.0	0.0	0.0
S02	KG/HR	0.0	0.0	0.0	0.0	57.0	0.0	0.0
H2SO4	KG/HR	0.0	0.0	0.0	0.0	0.0	0.0	0.0
O2	KG/HR	0.0	0.0	0.0	0.0	0.0	0.0	0.0
H2	KG/HR	0.0	14119.6	0.0	14119.6	14119.6	0.0	0.0
KS2	KG/HR	0.0	0.0	0.0	0.0	0.0	0.0	0.0
KS1	KG/HR	0.0	0.0	0.0	0.0	0.0	0.0	0.0
KPS	KG/HR	0.0	0.0	0.0	0.0	0.0	0.0	0.0
AHSS	KG/HR	0.0	0.0	0.0	0.0	0.0	0.0	0.0
AHSL	KG/HR	0.0	0.0	0.0	0.0	0.0	0.0	0.0
Mass Flow	KG/HR	10.3	14119.6	126579.0	14119.6	14558.5	15492900.0	15492900.0
Volume Flow	CUM/HR	1.3	19292.0	127.5	12208.9	174175.0	24018.7	24018.7
Temperature	C	800.0	25.0	25.0	160.5	25.0	430.0	820.0
Pressure	BAR	9.0	9.0	9.0	20.7	1.0	9.0	9.0
Vapor Fraction		1.0	1.0	0.0	1.0	1.0	0.0	0.0
Liquid Fraction		0.0	0.0	1.0	0.0	0.0	1.0	1.0
Solid Fraction		0.0	0.0	0.0	0.0	0.0	0.0	0.0
Average Molecular Weight		80.1	2.0	18.0	2.0	2.1	251.7	251.7

A.2. Mass flow rate stream table (continued)

	Units	K2SO4	K2SO4-2	KPSL	KS-KPS	KSL	LOWPROD	MIDPROD1
From		FDMIX	SEP-MID		SEP-LOW		LTR	MTR
To		LTR		FDMIX	SPT-KS	FDMIX	SEP-LOW	SEP-MID
Substream: MIXED								
Phase: All								
Component Mass Flow								
K2SO4	KG/HR	3594880.0	2406460.0	0.0	1538600.0	3594880.0	1538600.0	0.0
K2S2O7	KG/HR	63581100.0	12141600.0	63581100.0	66582100.0	0.0	66582100.0	0.0
NH4)2SO4	KG/HR	0.0	0.0	0.0	0.0	0.0	0.0	0.0
NH4)2S03	KG/HR	0.0	0.0	0.0	0.0	0.0	0.0	0.0
NH3	KG/HR	0.0	0.0	0.0	0.0	0.0	414468.0	0.0
H2O	KG/HR	0.0	0.0	0.0	0.0	0.0	241736.0	0.0
SO3	KG/HR	0.0	0.0	0.0	0.0	0.0	0.0	936515.0
S02	KG/HR	0.0	0.0	0.0	0.0	0.0	23599.6	0.0
H2SO4	KG/HR	0.0	0.0	0.0	0.0	0.0	0.0	0.0
O2	KG/HR	0.0	0.0	0.0	0.0	0.0	0.0	0.0
H2	KG/HR	0.0	0.0	0.0	0.0	0.0	0.0	0.0
KS2	KG/HR	0.0	0.0	0.0	0.0	0.0	0.0	0.0
KS1	KG/HR	0.0	0.0	0.0	0.0	0.0	0.0	0.0
KPS	KG/HR	0.0	0.0	0.0	0.0	0.0	0.0	0.0
AHSS	KG/HR	0.0	0.0	0.0	0.0	0.0	0.0	0.0
AHSL	KG/HR	0.0	0.0	0.0	0.0	0.0	0.0	0.0
Mass Flow	KG/HR	67176000.0	14548000.0	63581100.0	68120700.0	3594880.0	68800500.0	936515.0
Volume Flow	CUM/HR	112071.0	30581.3	93125.5	105608.0	6745.1	107532.0	120286.0
Temperature	C	430.0	800.0	430.0	430.0	430.0	430.0	840.0
Pressure	BAR	9.0	9.0	9.0	9.0	9.0	9.0	9.0
Vapor Fraction		0.0	0.0	0.0	0.0	0.0	0.0	1.0
Liquid Fraction		1.0	1.0	1.0	1.0	1.0	1.0	0.0
Solid Fraction		0.0	0.0	0.0	0.0	0.0	0.0	0.0
Average Molecular Weight		248.2	236.4	254.3	251.7	174.3	222.8	80.1

A.2. Mass flow rate stream table (continued)

	Units	MIDPROD2	NH3-C1	NH3-C2	NH3-C3	NH3-HOT	NH3-W	O2
From		MTR	TURBINE	CONDENSE	PUMP-2	SEP-LOW	SPT-NH3	SEP-ABS
To		SEP-MID	CONDENSE	PUMP-2	SPT-NH3	TURBINE	ABSORBER	
Substream: MIXED								
Phase: All								
Component Mass Flow								
K2SO4	KG/HR	2406460.0	0.0	0.0	0.0	0.0	0.0	0.0
K2S2O7	KG/HR	12141600.0	0.0	0.0	0.0	0.0	0.0	0.0
NH4)2SO4	KG/HR	0.0	0.0	0.0	0.0	0.0	0.0	0.0
NH4)2S03	KG/HR	0.0	0.0	0.0	0.0	0.0	0.0	0.0
NH3	KG/HR	0.0	414468.0	414468.0	414468.0	414468.0	414468.0	0.0
H2O	KG/HR	0.0	241736.0	241736.0	241736.0	241736.0	241736.0	0.0
SO3	KG/HR	8363.9	0.0	0.0	0.0	0.0	0.0	0.0
S02	KG/HR	0.0	23599.6	23599.6	23599.6	23599.6	23599.6	0.0
H2SO4	KG/HR	0.0	0.0	0.0	0.0	0.0	0.0	0.0
O2	KG/HR	0.0	0.0	0.0	0.0	0.0	0.0	112104.0
H2	KG/HR	0.0	0.0	0.0	0.0	0.0	0.0	0.0
KS2	KG/HR	0.0	0.0	0.0	0.0	0.0	0.0	0.0
KS1	KG/HR	0.0	0.0	0.0	0.0	0.0	0.0	0.0
KPS	KG/HR	0.0	0.0	0.0	0.0	0.0	0.0	0.0
AHSS	KG/HR	0.0	0.0	0.0	0.0	0.0	0.0	0.0
AHSL	KG/HR	0.0	0.0	0.0	0.0	0.0	0.0	0.0
Mass Flow	KG/HR	14556400.0	679804.0	679804.0	679804.0	679804.0	679804.0	112104.0
Volume Flow	CUM/HR	30592.0	3720440.0	909.4	909.6	247648.0	909.6	9649.5
Temperature	C	840.0	196.3	20.0	20.1	430.0	20.1	25.0
Pressure	BAR	9.0	0.4	5.0	10.0	9.0	10.0	9.0
Vapor Fraction		0.0	1.0	0.0	0.0	1.0	0.0	1.0
Liquid Fraction		1.0	0.0	1.0	1.0	0.0	1.0	0.0
Solid Fraction		0.0	0.0	0.0	0.0	0.0	0.0	0.0
Average Molecular Weight		236.1	17.8	17.8	17.8	17.8	17.8	32.0

A.2. Mass flow rate stream table (continued)

	Units	PHTOPROD	SFITH202	SFIT-H2O	SFITPRD2	SFITPROD	SO2-02-6	SO2-O2-1
From		PHOT-REC	PUMP-1	MIXER	SEP-ABS	ABSORBER	HTR	SPT-SO2
To		PHOTFLAS	PHOT-REC	PUMP-1	MIXER	SEP-ABS	SPT-SO2	HX-1
Substream: MIXED								
Phase: All								
Component Mass Flow								
K2SO4	KG/HR	0.0	0.0	0.0	0.0	0.0	0.0	0.0
K2S2O7	KG/HR	0.0	0.0	0.0	0.0	0.0	0.0	0.0
NH4)2SO4	KG/HR	1559220.0	633558.0	633558.0	633558.0	633558.0	0.0	0.0
NH4)2S03	KG/HR	42820.1	856402.0	856402.0	856402.0	856402.0	0.0	0.0
NH3	KG/HR	0.0	0.0	0.0	0.0	0.0	0.0	0.0
H2O	KG/HR	22899.1	149098.0	149098.0	22519.1	22519.1	0.0	0.0
SO3	KG/HR	0.0	0.0	0.0	0.0	0.0	383875.0	383874.0
S02	KG/HR	84.9	84.9	84.9	84.9	84.9	448888.0	448886.0
H2SO4	KG/HR	0.0	0.0	0.0	0.0	0.0	0.0	0.0
O2	KG/HR	0.0	0.0	0.0	0.0	112104.0	112104.0	112104.0
H2	KG/HR	14121.5	0.0	0.0	0.0	0.0	0.0	0.0
KS2	KG/HR	0.0	0.0	0.0	0.0	0.0	0.0	0.0
KS1	KG/HR	0.0	0.0	0.0	0.0	0.0	0.0	0.0
KPS	KG/HR	0.0	0.0	0.0	0.0	0.0	0.0	0.0
AHSS	KG/HR	0.0	0.0	0.0	0.0	0.0	0.0	0.0
AHSL	KG/HR	0.0	0.0	0.0	0.0	0.0	0.0	0.0
Mass Flow	KG/HR	1639140.0	1639140.0	1639140.0	1512560.0	1624670.0	944868.0	944864.0
Volume Flow	CUM/HR	26453.2	2238.8	2238.5	2235.9	11533.6	158800.0	158799.0
Temperature	C	79.7	25.3	25.0	25.0	25.0	850.0	850.0
Pressure	BAR	9.0	9.0	7.0	9.0	9.0	9.0	9.0
Vapor Fraction		0.3	0.0	0.0	0.0	0.2	1.0	1.0
Liquid Fraction		0.7	1.0	1.0	1.0	0.8	0.0	0.0
Solid Fraction		0.0	0.0	0.0	0.0	0.0	0.0	0.0
Average Molecular Weight		80.2	80.2	80.2	112.7	96.0	61.7	61.7

A.2. Mass flow rate stream table (continued)

	Units	SO2-O2-2	SO2-O2-3	SO2-O2-4	SO2-O2-5	SO3	SO3-1	SO3-2
From		HX-1	HX-2	HX-3	ABSCOLER	HX-1	SEP-MID	SPT-SO3
To		HX-2	HX-3	ABSCOLER	ABSORBER	HTR	SPT-SO3	HX-1
Substream: MIXED								
Phase: All								
Component Mass Flow								
K2SO4	KG/HR	0.0	0.0	0.0	0.0	0.0	0.0	0.0
K2S2O7	KG/HR	0.0	0.0	0.0	0.0	0.0	0.0	0.0
NH4)2SO4	KG/HR	0.0	0.0	0.0	0.0	0.0	0.0	0.0
NH4)2S03	KG/HR	0.0	0.0	0.0	0.0	0.0	0.0	0.0
NH3	KG/HR	0.0	0.0	0.0	0.0	0.0	0.0	0.0
H2O	KG/HR	0.0	0.0	0.0	0.0	0.0	0.0	0.0
SO3	KG/HR	383874.0	383874.0	383874.0	383874.0	944868.0	944878.0	944868.0
S02	KG/HR	448886.0	448886.0	448886.0	448886.0	0.0	0.0	0.0
H2SO4	KG/HR	0.0	0.0	0.0	0.0	0.0	0.0	0.0
O2	KG/HR	112104.0	112104.0	112104.0	112104.0	0.0	0.0	0.0
H2	KG/HR	0.0	0.0	0.0	0.0	0.0	0.0	0.0
KS2	KG/HR	0.0	0.0	0.0	0.0	0.0	0.0	0.0
KS1	KG/HR	0.0	0.0	0.0	0.0	0.0	0.0	0.0
KPS	KG/HR	0.0	0.0	0.0	0.0	0.0	0.0	0.0
AHSS	KG/HR	0.0	0.0	0.0	0.0	0.0	0.0	0.0
AHSL	KG/HR	0.0	0.0	0.0	0.0	0.0	0.0	0.0
Mass Flow	KG/HR	944864.0	944864.0	944864.0	944864.0	944868.0	944878.0	944868.0
Volume Flow	CUM/HR	155971.0	154993.0	132660.0	13196.1	119114.0	116999.0	116998.0
Temperature	C	830.0	823.1	665.1	25.0	819.4	800.0	800.0
Pressure	BAR	9.0	9.0	9.0	9.0	9.0	9.0	9.0
Vapor Fraction		1.0	1.0	1.0	0.3	1.0	1.0	1.0
Liquid Fraction		0.0	0.0	0.0	0.7	0.0	0.0	0.0
Solid Fraction		0.0	0.0	0.0	0.0	0.0	0.0	0.0
Average Molecular Weight		61.7	61.7	61.7	61.7	80.1	80.1	80.1

A.3. Mole fraction stream table

	Units	AM2SO4-1	AM2SO4-2	AM2SO422	BOTTOMS	EXCS-KPS	EXCS-NH3	EXCS-SO2
From			PHOTFLAS	HX-3	H2SEP	SPT-KS	SPT-NH3	SPT-SO2
To		LTR	HX-3					
Substream: MIXED								
Phase: All								
Component Mole Fraction								
K2SO4		0.000	0.000	0.000	0.000	0.033	0.000	0.000
K2S2O7		0.000	0.000	0.000	0.000	0.967	0.000	0.000
NH4)2SO4		0.879	0.879	0.879	0.000	0.000	0.000	0.000
NH4)2S03		0.027	0.027	0.027	0.000	0.000	0.000	0.000
NH3		0.000	0.000	0.000	0.000	0.000	0.638	0.000
H2O		0.093	0.093	0.093	0.960	0.000	0.352	0.000
SO3		0.000	0.000	0.000	0.000	0.000	0.000	0.313
S02		0.000	0.000	0.000	0.040	0.000	0.010	0.458
H2SO4		0.000	0.000	0.000	0.000	0.000	0.000	0.000
O2		0.000	0.000	0.000	0.000	0.000	0.000	0.229
H2		0.000	0.000	0.000	0.000	0.000	0.000	0.000
KS2		0.000	0.000	0.000	0.000	0.000	0.000	0.000
KS1		0.000	0.000	0.000	0.000	0.000	0.000	0.000
KPS		0.000	0.000	0.000	0.000	0.000	0.000	0.000
AHSS		0.000	0.000	0.000	0.000	0.000	0.000	0.000
AHSL		0.000	0.000	0.000	0.000	0.000	0.000	0.000
Average Molecular Weight		121.070	121.060	121.060	19.871	251.712	17.832	61.737

A.3. Mole fraction stream table (continued)

	Units	EXCS-SO3	H2	H20-FEED	H2-COMP	H2-H20	K2S207	K2S207-2
From		SPT-SO3	H2SEP		COMPRESS	PHOTFLAS	SPT-KS	HX-2
To			COMPRESS	MIXER		H2SEP	HX-2	MTR
Substream: MIXED								
Phase: All								
Component Mole Fraction								
K2SO4		0.000	0.000	0.000	0.000	0.000	0.033	0.033
K2S2O7		0.000	0.000	0.000	0.000	0.000	0.967	0.967
NH4)2SO4		0.000	0.000	0.000	0.000	0.000	0.000	0.000
NH4)2S03		0.000	0.000	0.000	0.000	0.000	0.000	0.000
NH3		0.000	0.000	0.000	0.000	0.000	0.000	0.000
H2O		0.000	0.000	1.000	0.000	0.003	0.000	0.000
SO3		1.000	0.000	0.000	0.000	0.000	0.000	0.000
S02		0.000	0.000	0.000	0.000	0.000	0.000	0.000
H2SO4		0.000	0.000	0.000	0.000	0.000	0.000	0.000
O2		0.000	0.000	0.000	0.000	0.000	0.000	0.000
H2		0.000	1.000	0.000	1.000	0.997	0.000	0.000
KS2		0.000	0.000	0.000	0.000	0.000	0.000	0.000
KS1		0.000	0.000	0.000	0.000	0.000	0.000	0.000
KPS		0.000	0.000	0.000	0.000	0.000	0.000	0.000
AHSS		0.000	0.000	0.000	0.000	0.000	0.000	0.000
AHSL		0.000	0.000	0.000	0.000	0.000	0.000	0.000
Average Molecular Weight		80.064	2.016	18.015	2.016	2.072	251.712	251.712

A.3. Mole fraction stream table (continued)

	Units	K2SO4	K2SO4-2	KPSL	KS-KPS	KSL	LOWPROD	MIDPROD1
From		FDMIX	SEP-MID		SEP-LOW		LTR	MTR
To		LTR		FDMIX	SPT-KS	FDMIX	SEP-LOW	SEP-MID
Substream: MIXED								
Phase: All								
Component Mole Fraction								
K2SO4		0.076	0.224	0.000	0.033	1.000	0.029	0.000
K2S2O7		0.924	0.776	1.000	0.967	0.000	0.848	0.000
NH4)2SO4		0.000	0.000	0.000	0.000	0.000	0.000	0.000
NH4)2S03		0.000	0.000	0.000	0.000	0.000	0.000	0.000
NH3		0.000	0.000	0.000	0.000	0.000	0.079	0.000
H2O		0.000	0.000	0.000	0.000	0.000	0.043	0.000
SO3		0.000	0.000	0.000	0.000	0.000	0.000	1.000
S02		0.000	0.000	0.000	0.000	0.000	0.001	0.000
H2SO4		0.000	0.000	0.000	0.000	0.000	0.000	0.000
O2		0.000	0.000	0.000	0.000	0.000	0.000	0.000
H2		0.000	0.000	0.000	0.000	0.000	0.000	0.000
KS2		0.000	0.000	0.000	0.000	0.000	0.000	0.000
KS1		0.000	0.000	0.000	0.000	0.000	0.000	0.000
KPS		0.000	0.000	0.000	0.000	0.000	0.000	0.000
AHSS		0.000	0.000	0.000	0.000	0.000	0.000	0.000
AHSL		0.000	0.000	0.000	0.000	0.000	0.000	0.000
Average Molecular Weight		248.221	236.361	254.324	251.712	174.260	222.834	80.064

A.3. Mole fraction stream table (continued)

	Units	MIDPROD2	NH3-C1	NH3-C2	NH3-C3	NH3-HOT	NH3-W	O2
From		MTR	TURBINE	CONDENSE	PUMP-2	SEP-LOW	SPT-NH3	SEP-ABS
To		SEP-MID	CONDENSE	PUMP-2	SPT-NH3	TURBINE	ABSORBER	
Substream: MIXED								
Phase: All								
Component Mole Fraction								
K2SO4		0.224	0.000	0.000	0.000	0.000	0.000	0.000
K2S2O7		0.774	0.000	0.000	0.000	0.000	0.000	0.000
NH4)2SO4		0.000	0.000	0.000	0.000	0.000	0.000	0.000
NH4)2S03		0.000	0.000	0.000	0.000	0.000	0.000	0.000
NH3		0.000	0.638	0.638	0.638	0.638	0.638	0.000
H2O		0.000	0.352	0.352	0.352	0.352	0.352	0.000
SO3		0.002	0.000	0.000	0.000	0.000	0.000	0.000
S02		0.000	0.010	0.010	0.010	0.010	0.010	0.000
H2SO4		0.000	0.000	0.000	0.000	0.000	0.000	0.000
O2		0.000	0.000	0.000	0.000	0.000	0.000	1.000
H2		0.000	0.000	0.000	0.000	0.000	0.000	0.000
KS2		0.000	0.000	0.000	0.000	0.000	0.000	0.000
KS1		0.000	0.000	0.000	0.000	0.000	0.000	0.000
KPS		0.000	0.000	0.000	0.000	0.000	0.000	0.000
AHSS		0.000	0.000	0.000	0.000	0.000	0.000	0.000
AHSL		0.000	0.000	0.000	0.000	0.000	0.000	0.000
Average Molecular Weight		236.096	17.832	17.832	17.832	17.832	17.832	31.999

A.3. Mole fraction stream table (continued)

	Units	PHTOPROD	SFITH202	SFIT-H2O	SFITPRD2	SFITPROD	SO2-02-6	SO2-O2-1
From		PHOT-REC	PUMP-1	MIXER	SEP-ABS	ABSORBER	HTR	SPT-SO2
To		PHOTFLAS	PHOT-REC	PUMP-1	MIXER	SEP-ABS	SPT-SO2	HX-1
Substream: MIXED								
Phase: All								
Component Mole Fraction								
K2SO4		0.000	0.000	0.000	0.000	0.000	0.000	0.000
K2S2O7		0.000	0.000	0.000	0.000	0.000	0.000	0.000
NH4)2SO4		0.577	0.235	0.235	0.357	0.283	0.000	0.000
NH4)2S03		0.018	0.361	0.361	0.549	0.436	0.000	0.000
NH3		0.000	0.000	0.000	0.000	0.000	0.000	0.000
H2O		0.062	0.405	0.405	0.093	0.074	0.000	0.000
SO3		0.000	0.000	0.000	0.000	0.000	0.313	0.313
S02		0.000	0.000	0.000	0.000	0.000	0.458	0.458
H2SO4		0.000	0.000	0.000	0.000	0.000	0.000	0.000
O2		0.000	0.000	0.000	0.000	0.207	0.229	0.229
H2		0.343	0.000	0.000	0.000	0.000	0.000	0.000
KS2		0.000	0.000	0.000	0.000	0.000	0.000	0.000
KS1		0.000	0.000	0.000	0.000	0.000	0.000	0.000
KPS		0.000	0.000	0.000	0.000	0.000	0.000	0.000
AHSS		0.000	0.000	0.000	0.000	0.000	0.000	0.000
AHSL		0.000	0.000	0.000	0.000	0.000	0.000	0.000
Average Molecular Weight		80.170	80.170	80.170	112.712	96.003	61.737	61.737

A.3. Mole fraction stream table (continued)

	Units	SO2-O2-2	SO2-O2-3	SO2-O2-4	SO2-O2-5	SO3	SO3-1	SO3-2
From		HX-1	HX-2	HX-3	ABSCOLER	HX-1	SEP-MID	SPT-SO3
To		HX-2	HX-3	ABSCOLER	ABSORBER	HTR	SPT-SO3	HX-1
Substream: MIXED								
Phase: All								
Component Mole Fraction								
K2SO4		0.000	0.000	0.000	0.000	0.000	0.000	0.000
K2S2O7		0.000	0.000	0.000	0.000	0.000	0.000	0.000
NH4)2SO4		0.000	0.000	0.000	0.000	0.000	0.000	0.000
NH4)2S03		0.000	0.000	0.000	0.000	0.000	0.000	0.000
NH3		0.000	0.000	0.000	0.000	0.000	0.000	0.000
H2O		0.000	0.000	0.000	0.000	0.000	0.000	0.000
SO3		0.313	0.313	0.313	0.313	1.000	1.000	1.000
S02		0.458	0.458	0.458	0.458	0.000	0.000	0.000
H2SO4		0.000	0.000	0.000	0.000	0.000	0.000	0.000
O2		0.229	0.229	0.229	0.229	0.000	0.000	0.000
H2		0.000	0.000	0.000	0.000	0.000	0.000	0.000
KS2		0.000	0.000	0.000	0.000	0.000	0.000	0.000
KS1		0.000	0.000	0.000	0.000	0.000	0.000	0.000
KPS		0.000	0.000	0.000	0.000	0.000	0.000	0.000
AHSS		0.000	0.000	0.000	0.000	0.000	0.000	0.000
AHSL		0.000	0.000	0.000	0.000	0.000	0.000	0.000
Average Molecular Weight		61.737	61.737	61.737	61.737	80.064	80.064	80.064

A.4. Heat, density and cost steam table

	Units	AM2SO4-1	AM2SO4-2	AM2SO422	BOTTOMS	EXCS-KPS	EXCS-NH3	EXCS-SO2
From			PHOTFLAS	HX-3	H2SEP	SPT-KS	SPT-NH3	SPT-SO2
To		LTR	HX-3					
Phase: All								
Mass Enthalpy	MJ/KG	-8.94815	-9.08153	-8.99698	-14.4611	-7.76045	-8.40823	-3.51853
Molar Enthalpy	MJ/HR	-1227.35	-1245.54	-1233.95	-325.553	-2213.04	-169.861	-246.096
Mass Entropy	J/KG-K	4266.386	3712.382	4085.993	-7972.03	3546.03	-10068.8	582.7006
Molar Entropy	J/KMOL-K	516531	449422	494651	-158410	892579	-179540	35974.08
Mass Density	KG/CUM	457.0811	465.5176	460.0801	1040.514	645.0353	747.3807	5.950068
Molar Density	KMOL/CUM	3.775348	3.845341	3.800425	52.36318	2.56259	41.91321	0.096378
Liquid Fraction		1	1	1	1	1	1	0
Vapor Fraction		0	0	0	0	0	0	1
Solid Fraction		0	0	0	0	0	0	0
Standard Volume Flow	CUM/KMOL	0.264537	0.26451	0.26451	0.019481	0.009752	0.04106	0.053558
Pressure	BAR	9	1	9	9	9	10	9
Temperature	C	110	25	80	25	430.0156	20.09547	849.9996
Total stream cost	$/SEC	0		0	0	0	0	

A.4. Heat, density and cost steam table (Continued)

	Units	EXCS-SO3	H2	H20-FEED	H2-COMP	H2-H20	K2S207	K2S207-2
From		SPT-SO3	H2SEP		COMPRESS	PHOTFLAS	SPT-KS	HX-2
To			COMPRESS	MIXER		H2SEP	HX-2	MTR
Phase: All								
Mass Enthalpy	MJ/KG	-4.28578	9.48E-10	-15.8745	1.930063	-0.37052	-7.76045	-7.76006
Molar Enthalpy	MJ/HR	-388.747	2.16E-09	-323.995	4.407927	-0.86976	-2213.04	-2212.93
Mass Entropy	J/KG-K	-221.939	-9007.98	-9063.3	-7107.12	76.29978	3546.03	3548.109
Molar Entropy	J/KMOL-K	-17769.3	-18159	-163280	-14327.1	158.0939	892579	893103
Mass Density	KG/CUM	8.075942	0.731889	993.0289	1.1565	0.083585	645.0353	645.0353
Molar Density	KMOL/CUM	0.100868	0.363062	55.12148	0.573695	0.04034	2.56259	2.56259
Liquid Fraction		0	0	1	0	0	1	1
Vapor Fraction		1	1	0	1	1	0	0
Solid Fraction		0	0	0	0	0	0	0
Standard Volume Flow	CUM/KMOL	0.053558	0.053558	0.01805	0.053558	0.053451	0.009752	0.009752
Pressure	BAR	9	9	9	20.68427	1	9	9
Temperature	C	800	25	25	160.4926	25	430.0156	820
Total stream cost	$/SEC	0		0.09177	13.72735			

A.4. Heat, density and cost steam table (Continued)

	Units	K2SO4	K2SO4-2	KPSL	KS-KPS	KSL	LOWPROD	MIDPROD1
From		FDMIX	SEP-MID		SEP-LOW		LTR	MTR
To		LTR		FDMIX	SPT-KS	FDMIX	SEP-LOW	SEP-MID
Phase: All								
Mass Enthalpy	MJ/KG	-7.76317	-7.72969	-7.75847	-7.76045	-7.84632	-7.73853	-4.24736
Molar Enthalpy	MJ/HR	-2183.11	-2069.84	-2235.44	-2213.04	-1549.04	-1953.61	-385.262
Mass Entropy	J/KG-K	3660.409	4129.566	3460.874	3546.03	7020.832	3473.52	-186.786
Molar Entropy	J/KMOL-K	908592	976068	880185	892579	1223450	774017	-14954.9
Mass Density	KG/CUM	599.4075	475.7156	682.7461	645.0353	532.9644	639.8126	7.785746
Molar Density	KMOL/CUM	2.414811	2.012666	2.684548	2.56259	3.05844	2.871256	0.097244
Liquid Fraction		1	1	1	1	1	1	0
Vapor Fraction		0	0	0	0	0	0	1
Solid Fraction		0	0	0	0	0	0	0
Standard Volume Flow	CUM/KMOL	0.022785	0.067064	0	0.009752	0.298906	0.013618	0.053558
Pressure	BAR	9	9	9	9	9	9	9
Temperature	C	430	800	430	430.0156	430	430.0156	839.9992
Total stream cost	$/SEC		0	0		0		

A.4. Heat, density and cost steam table (Continued)

	Units	MIDPROD2	NH3-C1	NH3-C2	NH3-C3	NH3-HOT	NH3-W	O2
From		MTR	TURBINE	CONDENSE	PUMP-2	SEP-LOW	SPT-NH3	SEP-ABS
To		SEP-MID	CONDENSE	PUMP-2	SPT-NH3	TURBINE	ABSORBER	
Phase: All								
Mass Enthalpy	MJ/KG	-7.72297	-6.21986	-8.40902	-8.40823	-5.67241	-8.40823	5.82E-17
Molar Enthalpy	MJ/HR	-2065.72	-125.652	-169.877	-169.861	-114.593	-169.861	2.11E-15
Mass Entropy	J/KG-K	4132.194	-2724.14	-10071.4	-10068.8	-3233.85	-10068.8	-567.49
Molar Entropy	J/KMOL-K	975595	-48575.8	-179590	-179540	-57664.8	-179540	-18159
Mass Density	KG/CUM	475.823	0.182721	747.503	747.3807	2.745039	747.3807	11.61754
Molar Density	KMOL/CUM	2.015379	0.010247	41.92007	41.91321	0.153942	41.91321	0.363062
Liquid Fraction		1	0	1	1	0	1	0
Vapor Fraction		0	1	0	0	1	0	1
Solid Fraction		0	0	0	0	0	0	0
Standard Volume Flow	CUM/KMOL	0.067041	0.04106	0.04106	0.04106	0.04106	0.04106	0.053558
Pressure	BAR	9	0.4	5	10	9	10	9
Temperature	C	839.9992	196.3491	20	20.09549	430.0156	20.09547	25
Total stream cost	$/SEC							3.113995

A.4. Heat, density and cost steam table (Continued)

	Units	PHTOPROD	SFITH202	SFIT-H2O	SFITPRD2	SFITPROD	SO2-02-6	SO2-O2-1
From		PHOT-REC	PUMP-1	MIXER	SEP-ABS	ABSORBER	HTR	SPT-SO2
To		PHOTFLAS	PHOT-REC	PUMP-1	MIXER	SEP-ABS	SPT-SO2	HX-1
Phase: All								
Mass Enthalpy	MJ/KG	-8.91377	-9.67769	-9.67801	-9.15945	-8.52741	-3.51853	-3.51853
Molar Enthalpy	MJ/HR	-809.6	-878.983	-879.012	-1169.6	-927.472	-246.096	-246.096
Mass Entropy	J/KG-K	3991.963	3992.574	3990.807	5030.238	4644.771	582.7006	582.7006
Molar Entropy	J/KMOL-K	320035	320084	319942	566969	445912	35974.08	35974.08
Mass Density	KG/CUM	61.96375	732.1538	732.2614	676.489	140.8638	5.950068	5.950068
Molar Density	KMOL/CUM	0.772907	9.132543	9.133887	6.001915	1.467284	0.096378	0.096378
Liquid Fraction		0.656112	1	1	1	0.800666	0	0
Vapor Fraction		0.343888	0	0	0	0.199334	1	1
Solid Fraction		0	0	0	0	0	0	0
Standard Volume Flow	CUM/KMOL	0.19198	0.077404	0.077404	0.10848	0.09711	0.053558	0.053558
Pressure	BAR	9	9	7	9	9	9	9
Temperature	C	79.73001	25.26923	25.00015	25	25	849.9996	849.9996
Total stream cost	$/SEC							

A.4. Heat, density and cost steam table (Continued)

	Units	SO2-O2-2	SO2-O2-3	SO2-O2-4	SO2-O2-5	SO3	SO3-1	SO3-2
From		HX-1	HX-2	HX-3	ABSCOLER	HX-1	SEP-MID	SPT-SO3
To		HX-2	HX-3	ABSCOLER	ABSORBER	HTR	SPT-SO3	HX-1
Phase: All								
Mass Enthalpy	MJ/KG	-3.53715	-3.54359	-3.68897	-4.56602	-4.26716	-4.28578	-4.28578
Molar Enthalpy	MJ/HR	-247.398	-247.848	-258.017	-319.36	-387.058	-388.747	-388.747
Mass Entropy	J/KG-K	565.9725	560.1213	416.9532	-1556.29	-204.743	-221.939	-221.939
Molar Entropy	J/KMOL-K	34941.34	34580.11	25741.36	-96080.3	-16392.6	-17769.3	-17769.3
Mass Density	KG/CUM	6.05794	6.096183	7.122423	71.60179	7.932466	8.075942	8.075942
Molar Density	KMOL/CUM	0.098125	0.098745	0.115368	1.159791	0.099076	0.100868	0.100868
Liquid Fraction		0	0	0	0.698463	0	0	0
Vapor Fraction		1	1	1	0.301537	1	1	1
Solid Fraction		0	0	0	0	0	0	0
Standard Volume Flow	CUM/KMOL	0.053558	0.053558	0.053558	0.053558	0.053558	0.053558	0.053558
Pressure	BAR	9	9	9	9	9	9	9
Temperature	C	830	823.0796	665.1285	25	819.4103	800	800
Total stream cost	$/SEC							